A Benchmark Experimental Database for Multiphase Combustion Model Input and Validation

JOHN F. WIDMANN and CARY PRESSER*
National Institute of Standards and Technology, Gaithersburg, MD 20899-8360, USA

Experimental data were obtained for the purpose of validating multiphase combustion models and submodels. A reference spray combustor was fabricated to permit well-defined input and boundary conditions, enabling measurements to characterize the fuel spray, combustion air, wall temperatures, gas temperatures, and species concentrations. The level of complexity of the reference spray combustor is consistent with a benchmark case in which the level of coupling between the flow field and the remaining physics (e.g., chemical reactions, heat transfer) is not as extensive as in the complete system, but is also not insignificant. The characteristics (i.e., size, velocity, volume flux, etc.) of the methanol fuel spray were determined using phase Doppler interferometry. Fourier transform infrared spectroscopy was used to measure the species concentrations in the reactor emissions, and the conversion of methanol in the reactor. Thermocouple measurements provide gas temperature data at the reactor exit. Particle image velocimetry was used to characterize the inlet combustion air, and also to provide validation data farther downstream.

INTRODUCTION

Control of process efficiency and the formation of undesirable byproducts from industrial thermal oxidation systems (e.g., power generation and treatment of liquid chemical wastes), is generally based on a priori knowledge of the input stream physical and chemical properties, desired stoichiometric conditions, and monitoring of a few major chemical species in the exhaust. Optimization of the performance of these systems is relying increasingly on computational models and simulations to provide relevant process information in a cost-effective manner. Although computational fluid dynamics (CFD) offers a cost-effective alternative to experiments, the accuracy of the CFD models must first be assured. This is accomplished by two means: verification and validation [1]. Verification involves ensuring that the algebraic and differential equations within the model have been accurately solved. In addition to verifying that the numerical code arrives at the correct solution, it is also necessary to determine if the correct model has been solved (i.e., that the physics has been accurately depicted). This is the validation step. The objective of this paper is to provide experimental data for multiphase combustion model and submodel validation.

The approach recommended by the American Institute of Aeronautics and Astronautics for validating CFD models of a complex system (e.g., burners, fluidized bed combustors) involves dividing the system of interest into three progressively simpler cases: *subsystem cases*, *benchmark cases*, and *unit problems* [1]. The objective is to determine the degree to which the model predictions compare with the experimental data at multiple levels of complexity. Subsystem cases represent the first level of simplification of the actual process. These cases commonly exhibit simplified geometries compared to the full-scale process.

The focus of this work is to provide experimental data at the benchmark case level. Benchmark cases represent the next level of decomposition of the complete system. The benchmark cases are geometrically simpler than, but represent key features of, the subsystem cases. The level of coupling between the flow field and the remaining physics (e.g., chemical reactions, heat transfer) is not as extensive as in the complete system, but is also not insignificant. The scope of the experimental measurements obtained in this phase is usually quite extensive, and the experimental uncertainties associated with those measurements are quantified. Unit problems represent the total decomposition of the complete system. Unit problems are characterized by very simple geometries and decoupling of the flow physics. Each phase of the validation process emphasizes certain features of the CFD

*Corresponding author. E-mail: cary.presser@nist.gov

COMBUSTION AND FLAME 129:47–86 (2002)

Published by Elsevier Science Inc.
0010-2180/02/$–see front matter
PII 0010-2180(01)00374-1

model. This paper presents a benchmark case suitable for validation of multiphase combustion models and submodels.

There is a dearth of databases of this kind, yet there is a need for such data by the spray combustion community. This database offers modelers a set of well-defined boundary and initial conditions, as well as downstream data that can be used for validation purposes. Many replicates of the measurements have been obtained over a period of time to enable statistical uncertainties to be specified for the data, operating conditions, and equipment, and to acquire the confidence of the modeling community. This paper follows a similar format to that recommended elsewhere [2, 3] to assure the usefulness of the data for model validation.

Measured Quantities

The experimental data presented herein correspond to a methanol spray flame within the research spray combustion facility at the National Institute of Standards and Technology (NIST). Data were obtained repeatedly over the course of several months under the same operating conditions to obtain measurement uncertainties. The operating conditions correspond to the baseline case of the database. Spray measurements were obtained non-intrusively using phase Doppler interferometry (PDI). Data are presented for the mean size, mean axial and radial components of velocity, number density, and volume flux of fuel droplets within the spray. The enclosed combustion chamber provides well-characterized boundary conditions, and wall temperature data are provided as a function of axial position. Gas temperature (using thermocouples) and species (using Fourier transform infrared spectroscopy) measurements were obtained at the reactor exit, and can be used for boundary conditions or validation of model predictions. To characterize the inlet combustion air, gas-phase velocity measurements were obtained using particle image velocimetry (PIV). The measurements reported herein constitute a database sufficiently complete for code validation, and several research groups have initiated simulations of the facility [4–7]. Metrology issues associated with the various diagnostics are discussed throughout this paper.

EXPERIMENTAL

Experimental Facility

Experiments were conducted in an enclosed spray combustion facility, shown in Fig. 1A. The experimental facility includes a swirl burner with a movable 12-vane swirl cascade. The cascade is adjusted to impart the desired degree of swirl intensity to the combustion air stream that passes through a 0.10 m diameter passage and co-flows around the fuel nozzle. Figure 1B presents a close-up view of the burner outlet and fuel nozzle. Note that the combustion air flows through an annulus located downstream of the swirl vanes before entering the reactor. The exit of the annulus, which surrounds the fuel line and nozzle, corresponds to the inlet of the reactor. The burner is shown at the base of the flame in the two photographs presented in Fig. 2. The photograph on the left shows the general shape and color of the flame. Because the lack of soot particles results in a flame that is not very luminous, the optical window on the far side of the reactor is visible in the photograph. The photograph on the right was obtained while the flame was illuminated with a laser light sheet from the Nd:YAG pulsed laser used for the PIV measurements. The fuel droplets are clearly visible in the photograph because of the elastically scattered laser light.

The liquid fuel is forced through a pressure-jet nozzle and forms a hollow-cone spray with a nominal 60° full cone angle. Methanol was used for these experiments, and the flow rate[1] was maintained at 3.0 kg h^{-1} ± 0.02 kg h^{-1}. The nominal upstream pressure of the liquid feed to the nozzle was maintained at 690 kPa. Methanol was chosen as the fuel because the thermodynamic and kinetic data necessary to model the gas-phase combustion are readily available [9], and the absence of soot in the flame reduces the complexity of the modeling effort. This reduced level of complexity is appropriate for benchmark cases, as discussed above. The fuel and combustion air were introduced into the reactor at room temperature. The flame is fired in a

[1]Unless otherwise stated, all uncertainties reported herein correspond to the combined expanded uncertainty, U_c, with a coverage factor, $k = 2$, and thus represent an approximate 95% confidence interval [8].

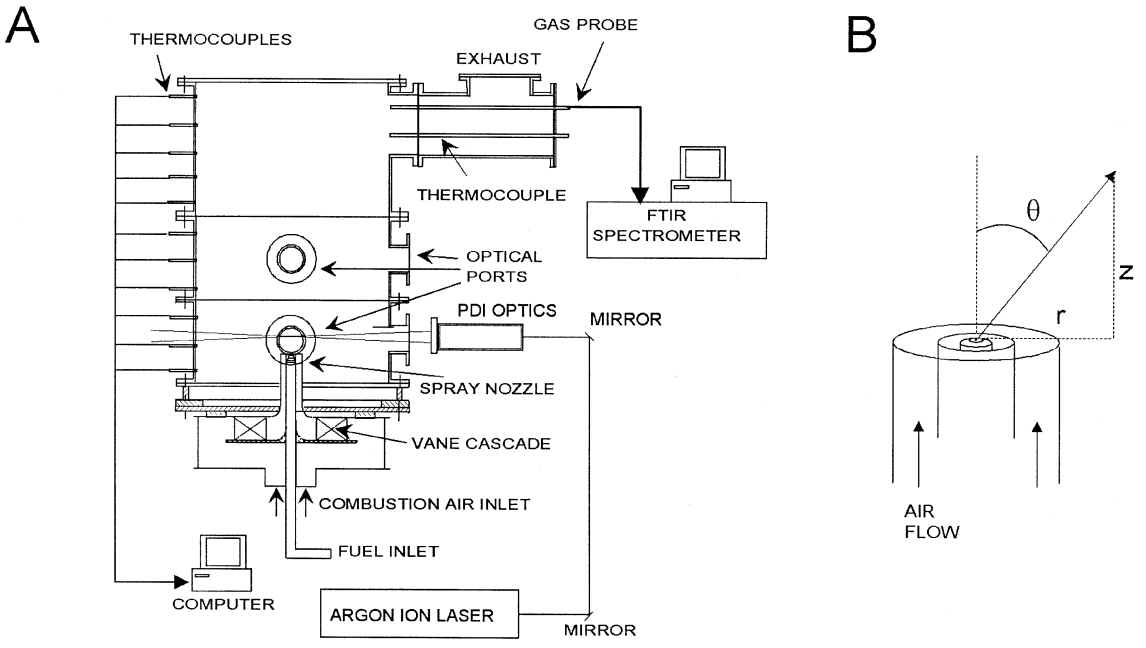

Fig. 1. Schematic of (A) the research spray combustion facility and (B) the atomizer nozzle and combustion air inlet.

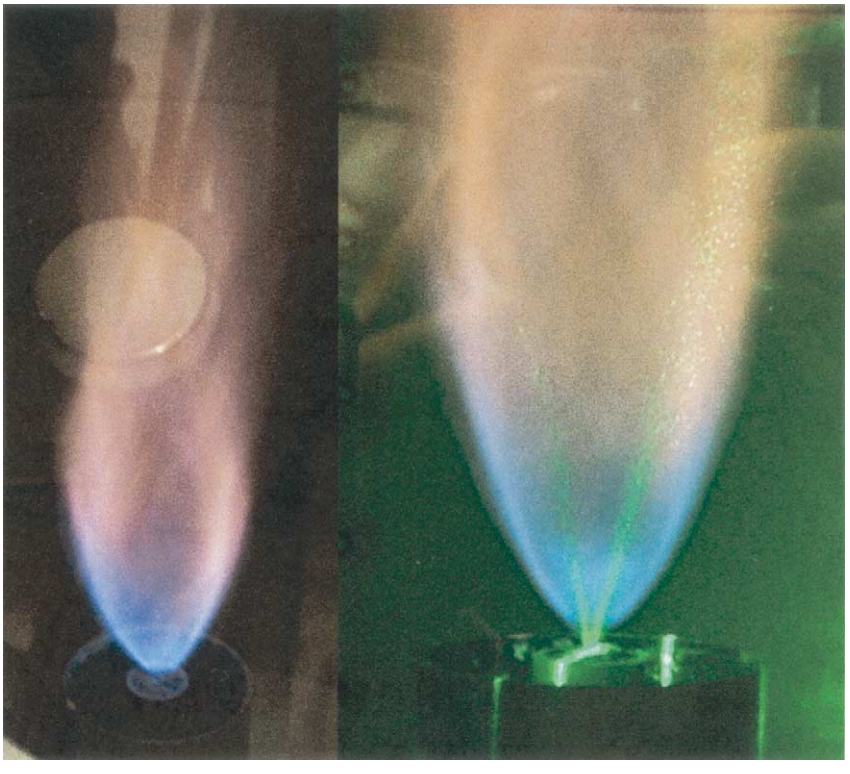

Fig. 2. Photographs of the methanol spray flame showing the color and shape of the flame. The photograph on the right was obtained while the flame was illuminated with a laser light sheet (wavelength at 532 nm).

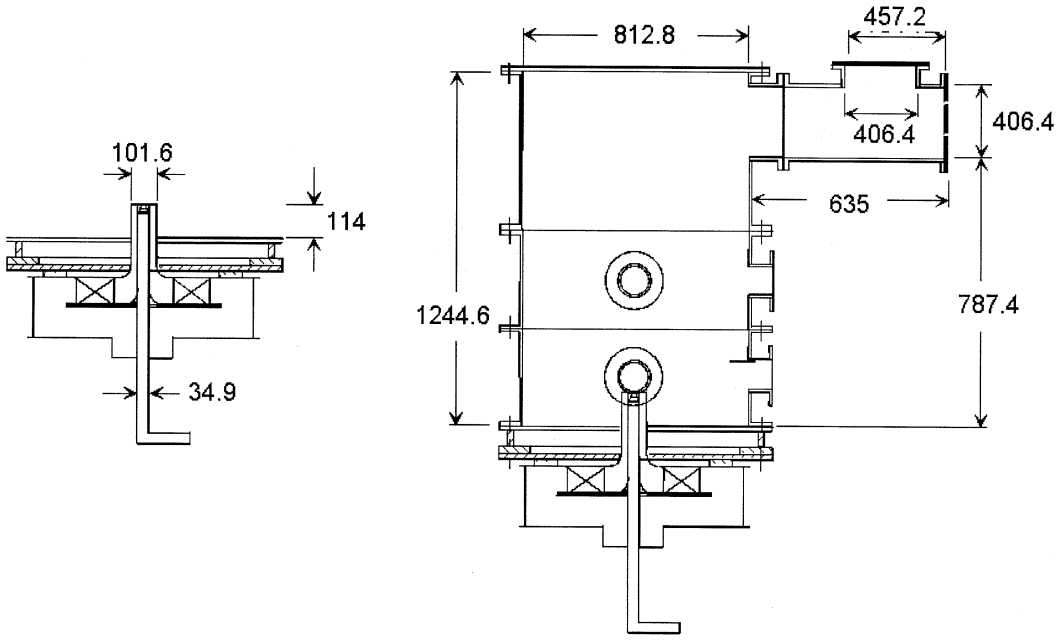

Fig. 3. Relevant dimensions in millimeters of the reactor and the burner.

vertical upwards configuration as shown in the photographs presented in Fig. 2. The fuel flow rate, combustion air flow rate, wall temperatures, and exiting gas temperatures were monitored continuously and stored using a computer-controlled data acquisition system.

The burner is enclosed within a stainless steel chamber to provide isolation from the ambient environment and improved control of the spray flame. The chamber height is 1.2 m and the inner diameter is 0.8 m. Several windows provide optical access for non-intrusive measurements. A stepper-motor-driven traversing system translates the entire burner/chamber assembly, permitting measurements of spray flame properties at selected locations downstream of the nozzle. Additional details on the design of the burner are available in Ref. [10]. The relevant dimensions necessary for modeling the facility are presented in Fig. 3. Note that the reactor exit is off-axis to permit direct probing of the flame, which makes the problem non-axisymmetric.

Diagnostics

The spray measurements were obtained using a two-component phase Doppler interferometry (PDI) system from Aerometrics).[2] The instrument is composed of the following components: (i) transmitter (model XMT-1100–4S), (ii) motor controller (model MCB-7100–1), (iii) receiver (model RCV-2100), (iv) counter-type signal processor (model PDP-3100), and (v) data management system (model DMS-4000–5). The PDI was controlled using Aerometrics PDPA software version 4.27J run on a 66 MHz personal computer. The receiving optics were aligned at a 30° scattering angle measured from the direction of propagation of the laser beams, and the transmitting and receiving optics were aligned at the same elevation. A 5 W argon ion laser operating in multi-line mode was used as the illumination source. The blue (wavelength = 488 nm) and green (wavelength = 514.5 nm) lines of the argon ion laser were separated and focused by the transmitting optics to intersect and form the probe volume. The transmitting and receiving optical systems both had front lenses with 500 mm focal lengths, and the receiver used a 100 μm slit aperture to limit

[2]Certain commercial equipment or materials are identified in this publication to specify adequately the experimental procedure. Such identification does not imply recommendation or endorsement by the National Institute of Standards and Technology, nor does it imply that the materials or equipment are necessarily the best available for this purpose.

the length of the probe volume. Details of the optical arrangement have been described previously [10, 11].

Gas-phase species concentrations were measured using Fourier transform infrared (FTIR) spectroscopy. An FTIR spectrometer (BioRad FTS-40) was used for extractive sampling of chemical species in the combustor emissions. A gas sampling system, consisting of an air-cooled sampling probe, heated gas line, and vacuum pump, facilitated the transport of the sample gas extracted from the spray combustor into the single-pass gas cell in a continuous manner. The sampling probe was designed to aerodynamically quench chemical reactions occurring within the gases being sampled [12]. The sampling gas line was also provided with a means for purging.

The design of the FTIR spectrometer is based upon the Michelson interferometer configuration. It consists of an infrared (IR) source, a beam splitter, two mirrors (one fixed in position and another movable), and an infrared detector. The source produces a beam of IR energy covering a broad range of infrared wavelengths. The beam is split into two using a beam splitter. One of these beams is directed to the fixed mirror while the other is directed to the movable mirror. The beams are reflected from the mirrors and recombined at the beam splitter. When the path-lengths of these two beams are not equal, the constructive and destructive interference results in an interferogram. The IR energy measured and plotted as a function of position of the movable mirror is the Fourier transform of IR energy intensity as a function of wavenumber. In practice, the absorption spectrum of a gas sample is obtained by passing the IR beam through a gas sample cell and measuring the energy intensity with an infrared detector.

In this investigation, the FTIR spectrometer was operated with 2 cm^{-1} resolution. The gas cell, equipped with KBr windows, was unheated and had a 0.1 m path length. The sample gas flows through the cell continuously exits. The pressure inside the cell was kept steady at a constant sub-atmospheric level. During operation, the sampling gas line was purged frequently with a stream of purified air. The data acquisition and analysis functions were accomplished with the software provided by the instrument vendor. In each test run, care was taken to allow sufficient time for equilibrating the flow and thereby assuring a steady state flow condition. Generally, three to five spectra were obtained at each probe location. Once the data acquisition at one location was completed the probe was removed and transferred to an adjacent location.

In each experiment, the gas-sampling probe was inserted into the exhaust gas stream as indicated in Fig. 1 to probe the conditions at the selected exit plane, about 0.53 m from the end plate and 0.51 m from the vertical axis of the combustion chamber. The extracted gas samples from each probe location were analyzed with the FTIR spectrometer and the spectral data were recorded. These spectra were used to identify the species present in the reactor emissions. Separately generated calibration spectra of each identified species was then used to quantify the species in the gas sample.

The inlet combustion air was characterized using a 3-D particle image velocimetry (PIV) system from Dantec, Inc. The PIV measurements require seed particles to be added to the flow, which are then assumed to follow the streamlines and act as tracers. The spatial displacement of the seed particles, corresponding to two images separated by a known time period, are measured and the velocity is deduced. The seed particles were nominally 1.5 μm aluminum oxide particles and were introduced into the combustion air upstream of the swirl vanes from a fluidized bed. The PIV images are obtained in a plane corresponding to the laser light sheet, and the time between the images is determined by the time between laser pulses. The spatial resolution of the PIV measurements depends directly upon the pixel resolution, field of view, and laser light sheet thickness, and indirectly on the seeding density. For the measurements presented here, the resolution is $\sim$1 mm. The 3-D PIV system differs from traditional PIV systems in that two CCD cameras are used, and three velocity components are measured [13].

A 50 mJ Nd:YAG laser was used as the illumination source for the PIV measurements. The pulse duration of the laser light sheet was $\approx$5 ns, and the wavelength of the light was 532 nm. A pair of 8-bit double-frame CCD cameras with a resolution of 1008 $\times$ 1018 pixels were used to obtain the images. The cameras were located at scattering angles of 87^{o} and 150^{o}, as measured from the direction of propagation of

TABLE 1

Operating Conditions for the Baseline Case

Fuel type	Methanol
Fuel flow rate	3.0 kg h^{-1}
Fuel temperature	Ambient
Equivalence ratio	0.3
Air flow rate	56.7 m^3 h^{-1}
Air temperature	Ambient
Vane angle	50°
Swirl number	0.58
Flame standoff distance	~5 mm
Chamber pressure	Ambient

the laser light sheet. Special camera mounts were utilized to permit the rotation of the camera body with respect to the camera lens to satisfy the Scheimpflug condition, which permits the laser sheet to be in focus despite the non-orthogonal camera alignment [13]. Bandpass filters (center wavelength = 532 nm, acceptance window = 30 nm) were used to reject the broadband radiation from the flame during the measurements. A conservative estimate of the dynamic range of the PIV measurements is 100:1.

Operating and Boundary Conditions

The operating conditions for the baseline case of the benchmark database are summarized in Table 1. The fuel flow rate into the reactor was measured using a turbine meter and maintained at 3.0 ± 0.02 kg h^{-1}. The rotation frequency of the turbine meter was calibrated as a function of the methanol flow rate, and the analog voltage signal from the turbine meter was read into the data acquisition system and calibrated as a function of the turbine frequency. Combining the calibration uncertainties with the variation observed from repeated measurements yields a combined expanded uncertainty of 0.0157 kg h^{-1} for the fuel flow rate. The individual components of the uncertainty budget are presented in Table A1 of the appendix.

TABLE 2

Reactor Wall Temperatures

Thermocouple	Height (mm)	Mean temperature (°C)
TC #1	99	93
TC #2	165	93
TC #3	231	95
TC #4	297	99
TC #5	429	103
TC #6	561	112
TC #7	693	114
TC #8	826	121
TC #9	958	133
TC #10	1090	136

TABLE 3

Exit Gas Temperatures

Radial coordinate, ρ (mm)	Polar angle, ϕ (deg)	Mean temperature (°C)
0	—	244
44.5	0	265
88.9	0	282
133.4	0	288
177.8	0	266
44.5	90	251
88.9	90	258
133.4	90	271
177.8	90	277
44.5	180	221
88.9	180	207
133.4	180	182
177.8	180	160

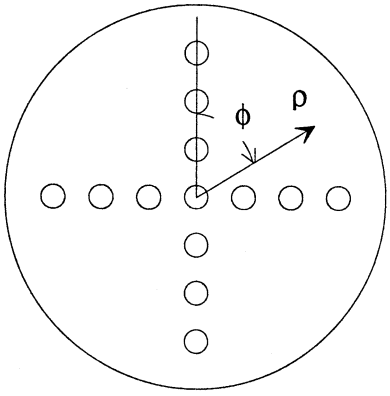

End Plate (see Fig. 1).

Sheathed K-type thermocouples (Omega Engineering, Inc.) were used to measure the wall temperatures and gas temperatures at the exit of the reactor. The locations and mean temperatures are summarized in Tables 2 and 3. The diameter of the Inconel sheath was 6.4 mm, and the time response of the thermocouples was ~2 s. The gas temperature at the exit plane of the reactor was measured at the same locations as the species concentration measurements. The exit plane is circular, and ρ and ϕ correspond to the

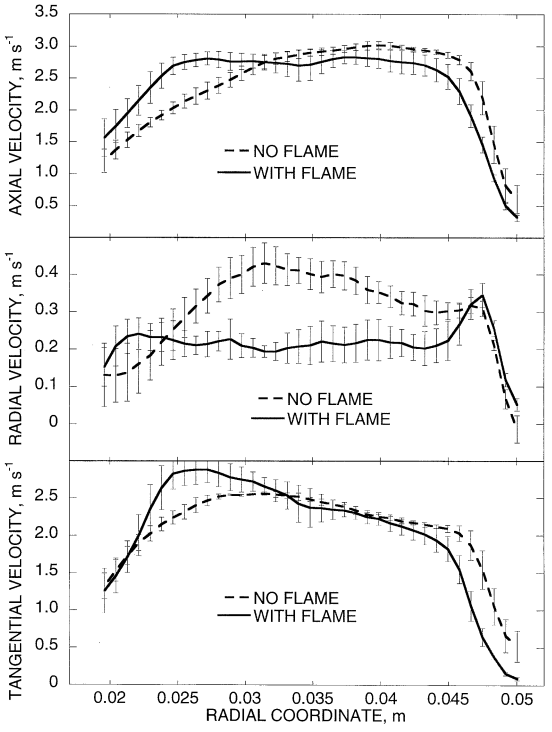

Fig. 4. Radial profiles of the three mean velocity components obtained from the PIV measurements. The profiles correspond to data obtained 1.4 mm downstream of the combustion air inlet with and without the spray flame present.

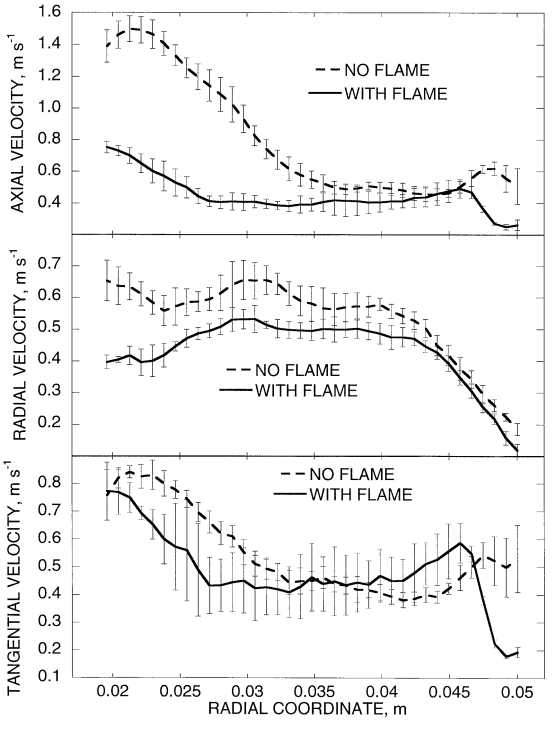

Fig. 5. Radial profiles of the fluctuations in the three velocity components obtained from the PIV measurements. The profiles correspond to data obtained 1.4 mm downstream of the combustion air inlet with and without the spray flame present.

distance from the center of the exit plane and the angle measured from vertical, respectively. The measurement uncertainties are 3°C and 5.5°C for the mean wall and gas temperatures, respectively.

The combustion air was delivered through the swirl burner at a rate of 56.7 $m^3\ h^{-1} \pm 1.7\ m^3\ h^{-1}$. The flow rate was measured using a 6.35 mm i.d. sonic nozzle for which the manufacturer reports a 3% uncertainty. This uncertainty is significantly larger than those associated with the calibration of the pressure transducer, the uncertainty of the pressure gauge, or the random errors determined from repeated measurements, which is shown in Table A2 of the appendix.

Inlet Combustion Air

Particle image velocimetry measurements of the gas-phase velocity were obtained to accurately characterize the inlet combustion air. Results from the PIV measurements are presented in Figs. 4-6 for the two cases in which the spray flame was and was not present. The axial, radial, and tangential mean velocity components are presented in Fig. 4. The velocity profiles presented in Fig. 4 were obtained at an axial location of 1.4 mm downstream of the combustion air inlet. This was determined to be sufficiently far from the reactor inlet that the velocity measurements were not biased by the annulus walls. It is interesting to note that the axial velocity profile peaks close to the outer wall of the annulus when there is no flame present. In contrast, when the flame is present, the profile is more uniform, suggesting that the buoyancy generated by the flame and drag that is attributed the spray reduces the pressure near the axis of the reactor, thus increasing the axial velocity in the region of the annulus close to the nozzle (as compared to the case without the flame). Also, larger values of the tangential velocity are measured near the reactor axis (i.e., toward the nozzle) when the spray flame is present.

The velocity fluctuations, u', for the three components of the inlet air velocity are presented in Fig. 5. The fluctuations of the axial velocity close

to the inner wall of the annulus (near the nozzle) for the case in which the spray flame is not present are considerably higher than the case with the flame. Presumably, this is because of the buoyancy induced by the flame and/or the momentum transfer between the spray and the surrounding gas, which was discussed above. Although the velocity fluctuations near the inner wall of the annulus are greater for the case without the flame for all three components of velocity, the data indicate that the effect of the flame on the radial and tangential velocity fluctuations is weaker than the effect on the fluctuations in the axial velocity component.

The uncertainty in the PIV measurements (error bars in Figs. 4 and 5) was estimated from the variation in the measurements (Type A uncertainty) and the PIV calibration (Type B uncertainty). The procedure of Taylor and Kuyatt [8] was used in computing the uncertainty in the experimental measurement. Uncertainties are classified as Type A or Type B, and it is assumed that the combined variance is the sum of the component variances. The Type A variance is a straightforward calculation based upon standard statistical methods applied to repeated measurements. The Type B uncertainties, which can not be quantified from replicated measurements, must be estimated using other means. For the case of the PIV measurements reported here, the uncertainty in the calibration was determined by measuring the velocity of a stationary calibration target. The mean error was greatest for the tangential velocity (0.014 m s^{-1}), with the error in the axial and radial velocities being considerably smaller (0.0002 m s^{-1} and 0.005 m s^{-1}, respectively). The uncertainty attributed to seeding density is more difficult to quantify, but has been estimated to be approximately $\pm$ 0.015 m s^{-1}. The calculated flow rate obtained by integrating the axial velocity profile over the combustion air inlet agrees with the total flow rate of air through the burner to within 1% (no flame present). The integrated flow rate for the case where the spray flame was present was also in agreement with the total flow through the burner to within the uncertainty in the measurements. The ability to close the mass balance provides confidence in the PIV measurements at the reactor inlet.

Figure 6 presents radial profiles of the three mean velocity components determined from the PIV measurements at the inlet and two downstream elevations within the reactor. The data correspond to velocity profiles with and without the flame present. Error bars have been omitted from the figure for clarity, but the uncertainty is consistent with the error bars in Fig. 4. The data can be used to compare with simulation predictions of the velocity field within the reactor with and without the flame present. The gas-phase velocity data corresponding to the cases with and without the spray flame are tabulated in Tables A3–A6 of the appendix.

Swirl Intensity

The degree of swirl (tangential momentum) present in the combustion air entering a burner or furnace has a strong effect on the structure and stability of the flame, and it is therefore an important parameter in the design and optimization of such systems. The swirl number, S, is a non-dimensional parameter that characterizes the degree of swirl present in the flow. It is defined as [14]

$$S = \frac{G_\theta}{LG_z} \tag{1}$$

where L is a characteristic length, typically chosen to be the exit radius of the burner. The terms G_θ and G_z are the axial flux of angular momentum and the axial flux of axial momentum, respectively, and are given by

$$G_\theta = \int_0^\infty \rho u_z u_\theta r^2 dr \tag{2}$$

and

$$G_z = \int_0^\infty (\rho u_z^2 + p) r dr. \tag{3}$$

Here u_z and u_θ are the axial and tangential velocity components, respectively. Also, $\int$ is the gas density, ρ is the gas pressure, and r is the radial coordinate. For the 12-vane-cascade swirl burner used here, the characteristic length was chosen as the radial coordinate of the outer wall of the annulus, L = 50.8 mm. The values of the swirl number, S, calculated from the PIV data are 0.58 and 0.60 for the cases with and without a spray flame, respectively. These values correspond to swirling flows of moderate intensity

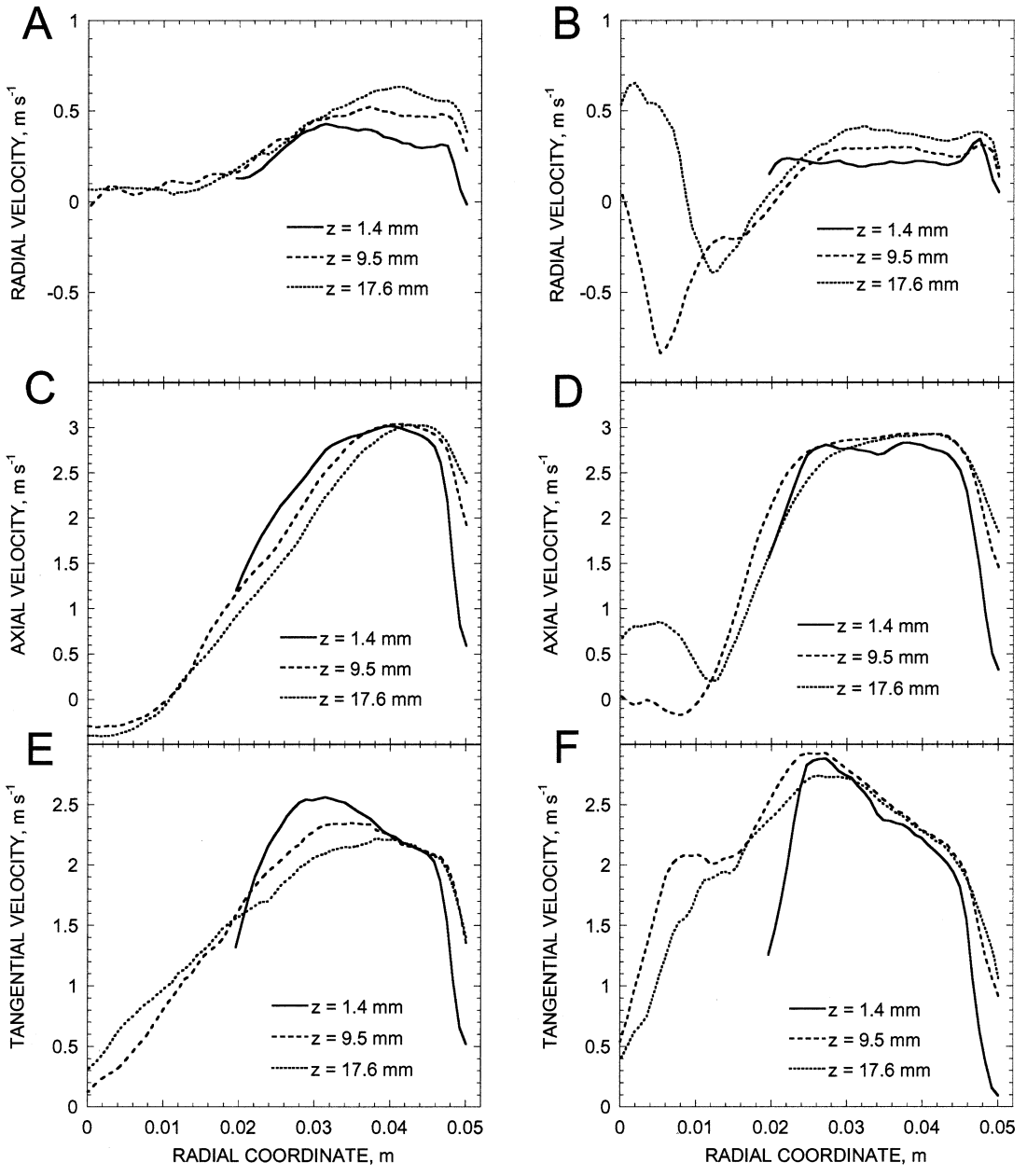

Fig. 6. Radial profiles of the three velocity components obtained from the PIV measurements at three downstream elevations within the reactor. The profiles correspond to data obtained (A, C, E) without the flame and (B, D, F) with the flame.

[14]. Note that the pressure term in Eq. 3 was omitted from the calculations because the pressure is unknown.

Fuel Spray

Figure 7A presents an example of droplet size data obtained at one location in the spray (axial coordinate, z = 5 mm; radial coordinate, r = 2.76 mm). Size distributions (probability density functions) from thirteen measurements (10,000 droplets per measurement) conducted on different days are shown. The data show good agreement over the thirteen experiments, with the largest variation in the probability density function occurring near a droplet diameter of ~15 μm. The data from Fig. 7A are shown in Fig. 7B with a cubic spline interpolation, which represents the mean size distribution. Figure 7C presents the

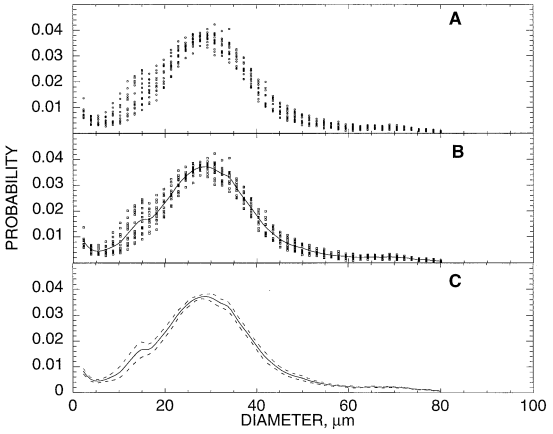

Fig. 7. Measured droplet size distributions at z = 5 mm and r = 2.76 mm. Presented are (A) the raw data from 13 experiments, (B) the raw data with the mean distribution obtained from a cubic spline interpolation, and (C) the cubic spline interpolation with the 95% pseudo-confidence bands.

mean distribution obtained from the cubic spline interpolation with pseudo-confidence bands that represent an approximate 95% confidence interval (Type A uncertainty only). The pseudo-confidence bands were calculated as $\pm 2sn^{-1/2}$, where s is the standard deviation of the raw data and n is the number of samples [11].

Experimental data were collected at seven elevations downstream of the nozzle (z = 5, 15, 25, 35, 45, 55, and 65 mm). These data are presented in Figs. 8-12 and are also tabulated in Tables A7 and A8 of the appendix. Furthermore, size (and velocity) distributions such as the one shown in Fig. 7C are available from the authors in electronic format at each location presented in Figs. 8 through 12. Droplet Sauter mean diameters, D_{32}, are presented in Fig. 8 for each of the seven downstream locations. The Sauter mean diameter is defined as [15]

$$D_{32} = \frac{\sum_i n_i d_i^3}{\sum_i n_i d_i^2}, \tag{4}$$

where n_i and d_i are the number of counts in, and the droplet diameter corresponding to, the i^{th} size class, respectively. Note that the number of counts in each size class, n_i, is corrected for the size dependence of the PDI probe volume [16]. Equation 4 corresponds to the conventional engineering definition, as opposed to the statistical definition of moments [17].

The mean axial and radial velocity components of the droplets are presented in Figs. 9 and 10, respectively. The mean axial velocity peaks at ~22 m s^{-1} in the most dense region of the spray at 5 mm downstream of the nozzle

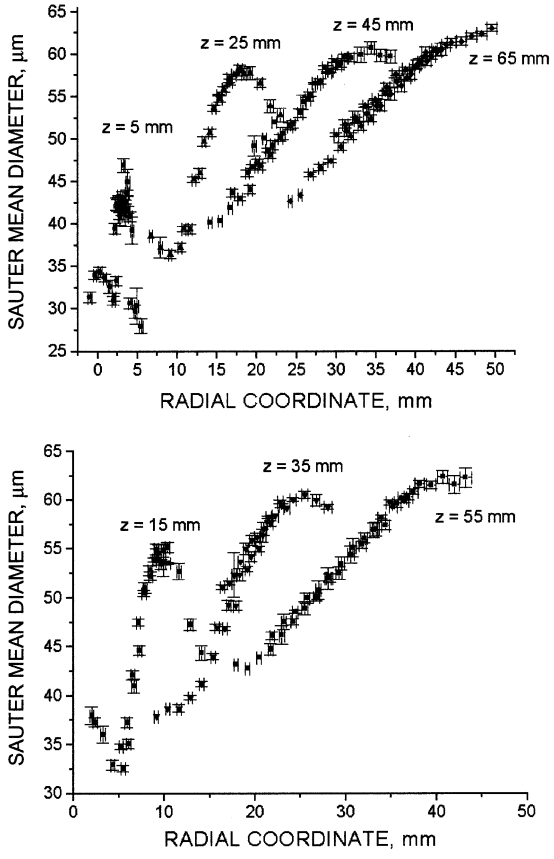

Fig. 8. Sauter mean diameter, D_{32}, at seven axial locations downstream of the nozzle (z = 5, 15, 25, 35, 45, 55, and 65 mm).

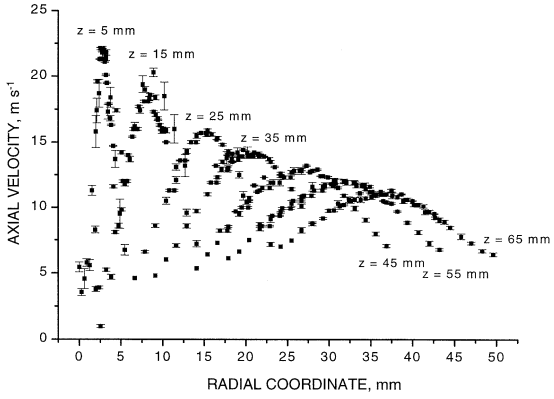

Fig. 9. Droplet mean axial velocity at seven axial locations downstream of the nozzle exit (z = 5, 15, 25, 35, 45, 55, and 65 mm).

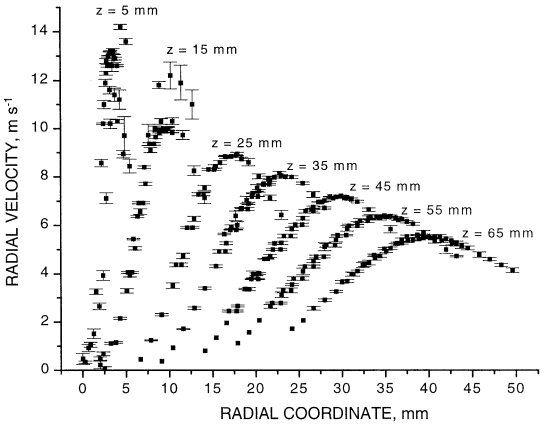

Fig. 10. Droplet mean radial velocity at seven axial locations downstream of the nozzle exit (z = 5, 15, 25, 35, 45, 55, and 65 mm).

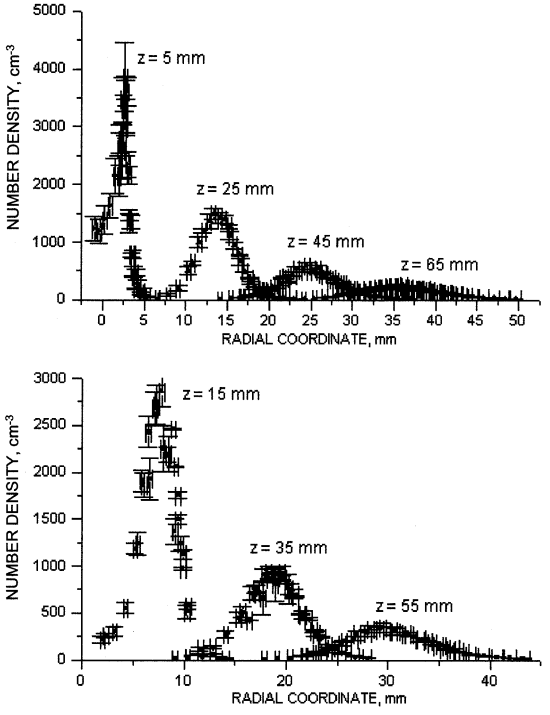

Fig. 11. Droplet number density at seven axial locations downstream of the nozzle exit (z = 5, 15, 25, 35, 45, 55, and 65 mm).

exit. The droplet velocities decrease moving further downstream, with a peak axial velocity of ~12 m s^{-1} at 65 mm downstream of the nozzle exit. The mean radial velocity profiles show similar behavior with a peak radial velocity at z = 5 mm of ~13 m s^{-1}. The peak radial velocity is reduced to roughly 6 m s^{-1} at z = 65 mm.

Figure 11 presents droplet number densities measured with the PDI at the downstream locations corresponding to the data shown in Figs. 9 and 10. The volume flux of fuel droplets corresponding to the same locations is shown in Fig. 12. The horizontal error bars express the uncertainty in the radial coordinate, and the vertical error bars correspond to twice the standard error of the mean ($2sn^{-1/2}$). The systematic errors associated with the instrument (Type B uncertainties) are not included in the figures but should be considered when comparing the data to numerical predictions. Type B uncertainties, which can be difficult to quantify, are discussed below. It should be noted that integrating the mass flux profiles over horizontal planes at z = 5 mm and z = 15 mm downstream of the nozzle indicates that the PDI measurements at these locations are not accounting for all of the fuel flowing through the nozzle [11]. This is a common problem for PDI measurements obtained close to the nozzle because of the very high number density of droplets in this region of the spray.

Many factors contribute to the uncertainties in PDI measurements, and Sellens [18], Widmann [19], and Friedman and Renksizbulut [20] have presented discussions of these factors. Sellens estimated that the systematic uncertainties for the system he used were 4% and 3% for the velocity and size measurements, respectively. These uncertainties are lower than those reported by Bulzan [21], who used a system similar to the one used for the experiments reported here. Bulzan estimated the droplet size uncertainty in an isothermal monodisperse droplet stream to be 6.5%, and noted that it would probably be larger in an evaporating, polydisperse spray. His estimate for the uncertainty in the velocity measurement was 10%. Widmann [19] noted that the uncertainty in the size and velocity measurements was dependent upon the fringe spacing in the probe volume, and that optimizing the optical system for one measurement could result in increased uncertainty in the other.

McDonell and Samuelsen [22] reported that the size error attributed to variation in the refractive index of a methanol spray when the temperature was varied from room temperature to the full boiling point. Taylor et al. [23] examined the errors associated with PDI mea-

surements using monodisperse polystyrene latex (PSL) spheres ranging in diameter (dp) from 0.7 μm to 10 μm. They found the systematic relative error of the instrument to be a strong function of particle size, with errors greater than 50% for $d_p = 0.7$ μm and errors in the range 7% - 14% for PSL spheres with $d_p > 1$ μm.

When using diagnostic techniques based upon laser light scattering in flames, there is the possibility that local variations in the refractive index, resulting from temperature and concentration variations, can result in beam steering. Taylor et al. investigated beam steering in flames and reported that the effect on PDI measurements is not critical. Beam steering may cause a loss of signal resulting in number density and volume flux measurements that are too low; however, this is not expected to introduce significant errors into the size and velocity measurements. We estimate the Type B uncertainty in the PDI measurements reported here to be 7.5% and 10.1% for the mean size and velocity measurements, respectively [11, 24]. It should be noted that the uncertainty in size and velocity *distributions* are generally higher than the uncertainty in measurements of individual droplets for numerous reasons, such as missed droplets, split Doppler bursts, and errors in the quantification of the probe area as a function of droplet size. These sources of uncertainty are discussed below in connection with the droplet number density and volume flux measurements.

The uncertainties associated with droplet number density and flux measurements deserve additional attention because of the difficulty in their quantification and their importance in satisfying mass conservation. Accurate droplet number density and volume flux measurements are difficult to make because they require accurate measurements of droplet size, droplet velocity, and probe volume dimensions. The dimensions of the probe volume are a function of the droplet diameter because of the Gaussain intensity profile of the laser beams and the droplet size dependence of the scattered light intensity [11, 16, 18–22]. The PDI software attempts to correct for the droplet size dependence; however, the manufacturer reports an uncertainty of 7.5% in determining the sample volume [25]. In addition, multiple particles may occupy the probe volume simultaneously, resulting in the signal being rejected or only one droplet being counted; thus, the number density and volume flux would be under-reported. An additional difficulty in quantifying the uncertainty of the volume flux and number density measurements is the possibility that Doppler signals may be split into multiple signals because of attenuation of the transmitting laser beams, which results in overcounting of the droplets [26–29].

Zhu et al. [30] discussed the difficulties of measuring simultaneously number densities and volume fluxes using PDI. Simultaneous measurements of the number density and volume flux is particularly difficult because the number density is dominated by the many small droplets while the volume flux is strongly dependent on the larger droplets. Therefore, if the size range of the droplets in the spray is greater than the dynamic range of the instrument (35:1 for the PDI processor used in this study), the simultaneous measurement of number density and volume flux will be very challenging.

As discussed above, the accuracy of both number density and volume flux measurements depends on several factors including the dynamic range of the instrument and accurately determining the probe volume. The dynamic range of the instrument is limited by the range of the photomultiplier tube detectors, which is considerably less than the dynamic range of the optical system [25, 31]. There are three main factors that contribute to uncertainties in the probe volume dimensions. The first is the variation of the probe diameter with droplet size. The probe volume can be approximated as a cylinder, where the laser beams determine the diameter and the length is determined by an aperture in the receiving optics (the system used here contains a 100 μm slit aperature). The effective diameter of the laser beam depends on the droplet size because larger droplets scatter significantly more light than smaller droplets [32]. Smaller droplets must pass through the center of the probe volume where the laser light intensity is higher, while larger droplets can scatter sufficient light to be detected when passing through the wings of the Gaussain intensity profile. Therefore, the probe volume diameter is larger for the larger droplets than for the smaller ones, and this size dependence must be considered when processing PDI data [16, 18–22, 30–31, 33].

The second factor contributing to the uncertainty in the probe volume is the error associ-

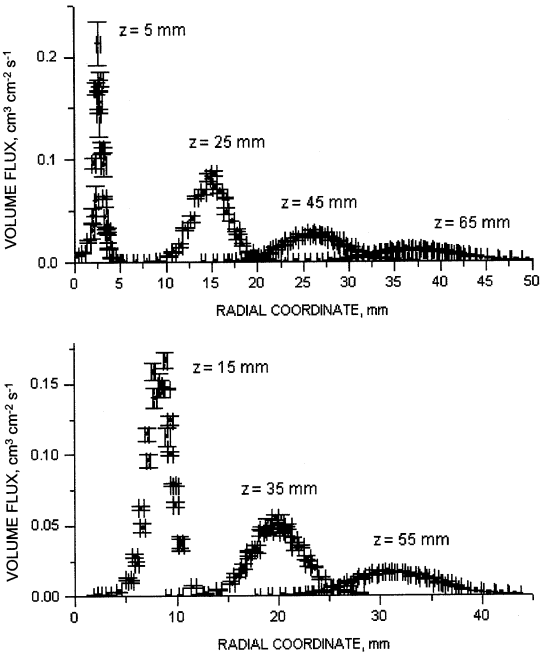

Fig. 12. Droplet volume flux at seven axial locations downstream of the nozzle exit (z = 5, 15, 25, 35, 45, 55, and 65 mm).

ated with measuring its length. The accuracy with which this dimension can be measured depends upon the resolution of the receiver optical system. Bachalo et al. [16] estimated this uncertainty to be 15% for a 100 μm slit; however, they note that larger particles will produce greater uncertainty in this dimension. The third factor that can contribute to the uncertainty in the probe volume is the particle trajectory. It is known that when the droplets have a component of velocity in the direction of the laser beams (the direction that is not measured when using a 2-component PDI system), the probe volume determined by the PDI software will be in error [16]. Unfortunately, the magnitude of this error is difficult to determine. For the spray investigated in this study, the swirling motion within the nozzle results in the droplets having a non-negligible tangential component of velocity near the nozzle exit, but this component is significantly reduced further downstream [34]. This may result in errors in number density and volume flux measurements close to the nozzle exit, for example, $z < 20$ mm.

A final factor that should be considered when assessing the accuracy of PDI volume flux measurements is that the volume flux is a vector quantity, but the PDI software reports a scalar measurement. The PDI software calculates the total volume of droplets passing through the probe volume regardless of the direction in which the droplets are moving. Instances in which this will lead to erroneous measurements include (1) recirculation zones and highly turbulent flow fields in which some droplets have positive velocities and other droplets have negative velocities, and (2) sprays where different size droplets move in different directions. A commercial PDI system that calculates a probe area for each velocity component, and thus, the corresponding components of the volume flux, has only recently become available [35].

A noteworthy conclusion of Friedman and Renksizbulut's analysis is that because of the large uncertainties, and the difficulty in their quantification, volume flux measurements should be used in a qualitative fashion rather than quantitatively. Because the volume flux measurements in the high number density region close to the nozzle are unreliable, it is common practice when modeling spray combustors to scale the volume flux profile at the inlet (i.e., z = 5 mm in Fig. 11) so that the integrated flow rate is consistent with the total flow rate of fuel through the nozzle [7].

Exhaust Chemical Species

The absorption spectra obtained with the FTIR spectrometer indicate that combustion was incomplete. Major species identified include CO_2, CO, and CH_3OH. No minor components or reaction intermediates were identified, perhaps because of the short instrument path length and the extractive nature of the measurement. Figure 13 presents the mole fraction of CO_2, CO, and CH_3OH at the exit plane of the reactor. The open and closed symbols correspond to vertical and horizontal profiles, respectively. The experimental data are also tabulated in Table A9 of the appendix in a format more easily used for comparison with simulation predictions.

The species concentrations are fairly uniform across the reactor exit plane. The variation in the replicated measurements is greater for the horizontal profiles than for the vertical profiles. The cause of the greater variation in the horizontal direction is unclear, but it may be attributed to "dead" regions in the exhaust passage in which the mixing is less pronounced and more sporadic.

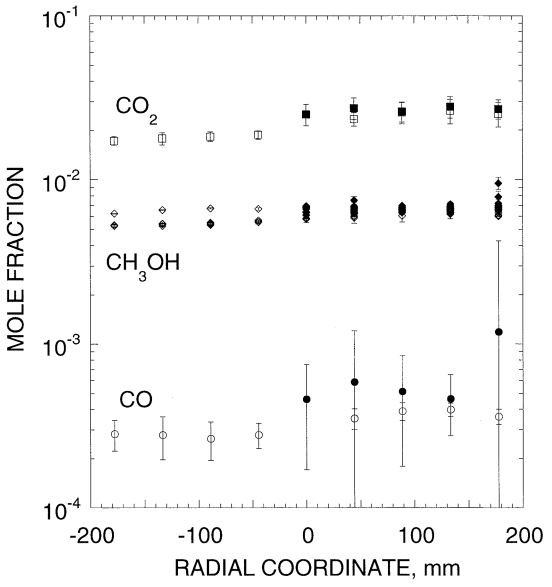

Fig. 13. The exit concentrations of various species in the reactor. Open and closed symbols correspond to vertical and horizontal profiles, respectively.

Note also that the concentration of CO_2 in the exhaust is ~50 times greater than that of CO, which indicates that the overall rate of methanol conversion to CO_2 and H_2O is occurring at a rate ~50 times faster than the overall conversion to CO and H_2O. The data presented in Fig. 13 result in an overall rate of methanol consumption in the reactor of 80% of the inlet fuel [24]. The incomplete conversion of the fuel spray provides an additional challenge for the simulations.

Summary

Experimental data were obtained from a reacting methanol spray under well-controlled conditions for the purpose of validating multiphase combustion models and submodels. Input and boundary conditions are provided for the defined baseline case. Droplet size and velocity distributions, number densities, and volume fluxes were measured using phase Doppler interferometry. Gas-phase species measurements were made using FTIR spectroscopy, and provide exhaust concentrations of CO, CO_2, and CH_3OH. The temperature of the reactor walls and the exhaust temperature are also provided.

The inlet combustion air was characterized using particle image velocimetry. The PIV data provide the measures of mean and fluctuating velocity components for the axial, radial, and tangential velocities, permitting calculation of the directional turbulence intensities and stresses. Much of the experimental data has been tabulated in the appendix, and all of the data are available in electronic format from the authors for parties interested in using the database to validate multiphase combustion models.

The authors would like to thank the following people who have contributed to the development of the NIST benchmark database for input and validation of multiphase combustion models: S. Rao Charagundla (NIST), Stefan D. Leigh (NIST), Alan Heckert (NIST), George Papadopolous (Dantec Dynamics), Mike Carrier (NIST), Jim Allan (NIST), Mike Hall (NIST), and Ashwani K. Gupta (University of Maryland).

REFERENCES

1. Oberkampf, W. L., Sindir, M. M., and Conlisk, A. T., Guide for the Verification and Validation of Computational Fluid Dynamics Simulations. *Am. Institute of Aeronautics and Astronautics*. Guide G-077–98, 1997.
2. McDonell, V. G., and Samuelsen, G. S., *J. Fluids Engineering* 117:145 (1995).
3: Faeth, G. M., and Samuelsen, G. S., *Prog. Energy Combust. Sci.* 12:305 (1986).
4. Gmurczyk, G., Presser, C., and Gupta, A. K., CFD Modeling of Spray Flames in an Enclosure. *Proceedings of the 1997 International Joint Power Generation Conference*. Vol. 1, EC-Vol. 5 (A. Sanyal, A. K. Gupta, and J. Veilleux, Eds.), pp. 399–410, ASME, New York, NY, 1997.
5. Giridharan, M. G., Sheu, J. C., Bayyuk, S., and Presser, C., An Unstructured Mesh Methodology for Computation of Reacting Sprays in Industrial Combustors. *Proceedings of the ASME Heat Transfer Division*, HTD-Vol. 364–2 (L. C. Witte, Ed.), pp. 433–441, Am. Society of Mechanical Engineers, NY, 1999.
6. Crocker, D. S., Giridharan, M. G., Widmann, J. F., and Presser, C., Simulation of Methanol Combustion in the NIST Reference Spray Combustor: *Proceedings of Combustion, Fire, and Computational Modeling of Industrial Combustion Systems,* FACT-Vol. 23, HTD-Vol. 367 (C. Presser, and A. K. Gupta, Eds.), pp. 95–102, ASME, New York, NY, 2000.
7. Crocker, D. S., Giridharan, M. G., Widmann, J. F., and Presser, C., Issues Related to Spray Combustion Modeling Validation. *AIAA Thirty-ninth Aerospace Science Meeting & Exhibit*, Reno, NV, January 8–11, 2001.
8. Taylor, B. N., and Kuyatt, C. E., Guidelines for Evaluating and Expressing the Uncertainty of NIST Measurement Results. NIST Technical Note 1297, National Institute of Standards and Technology, Gaithersburg, MD, September 1994.

9. Afeefy H. Y., Liebman J. F., and Stein S. E., Neutral Thermochemical Data in NIST Chemistry WebBook, NIST Standard Reference Database Number 69, Eds. W. G. Mallard, and P. J. Linstrom, March 1998, National Institute of Standards and Technology, Gaithersburg MD, 20899.
10. Presser, C., Gupta, A. K., Avedisian, C. T., and Semerjian, H. G., *Atomization and Sprays.* 4:207 (1994).
11. Widmann, J. F., Charagundla, S. R., Presser, C., and Heckert, A., Benchmark Experimental Database for Multiphase Combustion Model Input and Validation: Baseline Case –Progress Report. National Institute of Standards and Technology Internal Report No. 6286, 1999.
12. McVey, J. B., and Kennedy, J. B., *J. Energy* 4:32 (1980).
13. Flowmap® 3D-PIV System Owner's Manual, Dantec Measurement Technology, Inc., Mahwah, NJ, July 1999.
14. Gupta, A. K., Lilley, D. G., and Syred, N., *Swirl Flows.* Abacus Press, Kent, England (1984).
15. Mugele, R. A., and Evans, H. D., *Ind. Eng. Chem.* 43:1317 (1951).
16. Bachalo, W. D., Rudoff, R. C., and Brena de la Rosa, A., Mass Flux Measurements of a High Number Density Spray System Using the Phase Doppler Particle Analyzer, *AIAA Twenty-sixth Aerospace Sciences Meeting & Exhibit*, January 11–14, Reno, NV, 1998.
17. Sowa, W. A., *Atomization and Sprays* 2:1 (1992).
18. Sellens, R. W., Phase-Doppler Measurements Near the Nozzle in a Low-Pressure Water Spray, *Liquid Particle Size Measurement Techniques. 2nd Volume, ASTM STP 1083* (E. D. Hirleman, W. D. Bachalo, and P. G. Felton, Eds.) pp. 193–208. ASTM, Philadelphia, PA, 1990.
19. Widmann, J. F., *Atomization and Sprays*, 12:211 (2001).
20. Friedman, J. A., and Renksizbulut, M., *Combust. Flame* 117:661 (1999).
21. Bulzan, D. L., *J. Prop. Power*. 11;1093 (1995).
22. McDonell, V. G., and Samuelsen, G. S., *Combust. Sci. Tech.* 74:343 (1990).
23. Taylor, P., Dudek, R., Flaherty, D., and Kaempfe, T., *J. Aerosol Sci.* 25:419 (1994).
24. Widmann, J. F., Charagundla, S. R., and Presser, C., Benchmark Data for Fuel Atomization and Combustion Models. *Second International Symposium on Computational Technologies for Fluid/Thermal/Chem Systems with Industrial Applications.* Boston, MA, August 1–5, 1999.
25. Phase Doppler Particle Analyzer Owner's Manual, Aerometrics Inc., 1987.
26. Lazaro, B. J., Evaluation of Phase Doppler Particle Sizing in the Measurement of Optically Thick, High Number Density Sprays. UTRC91–11, United Technologies Research Center, East Hartford, CT, 1991.
27. Van Den Moortel, T., Santini, R., Tadrist, L., and Pantaloni, J., *Int. J. Multiphase Flow* 23:1189–1209 (1997).
28. Widmann, J. F., Presser, C., and Leigh, S. D., Effect of Burst-Splitting Events on Phase Doppler Interferometry Measurements. AIAA 2001–1130, *Thirty-ninth AIAA Aerospace Sciences Meeting & Exhibit*, Reno, NV, January 8–11, 2001.
29. Widmann, J. F., Presser, C., and Leigh, S. D., *Atomization and Sprays*, 11:717, (2001).
30. Zhu, J. Y., Rudoff, R. C., Bachalo, E. J., and Bachalo, W. D., Number Density and Mass Flux Measurements Using the Phase Doppler Particle Analyzer in Reacting and Non-Reacting Swirling Flows, *Thirty-first Aerospace Sciences Meeting & Exhibit*, Reno, NV, January 11–14, 1993.
31. Widmann, J. F., Charagundla, S. R., Presser, C., and Leigh, S. D., Splicing Together Size Distributions to Increase the Size Range of a Phase Doppler Interferometer, *Eighth International Conference on Liquid Atomization and Spray Systems*, pp. 687–690 (on CD), Pasadena, CA, July 2000.
32. van de Hulst, H. C., *Light Scattering by Small Particles*. John Wiley, New York, NY, 1957.
33. Widmann, J. F., Presser, C., and Leigh, S. D., *Measurement Sci. Technol.* 12:1180 (2001).
34. Presser, C., Gupta, A. K., and Semerjian, H. G., *Combust. Flame* 92:25 (1993).
35. Berkner, L., Fandrey, C., Miller, S., Naqwi, A., and Zhang, H., An Advanced Measurement System for Laser Doppler and Phase Doppler Applications. *Fourteenth Annual Conference on Liquid Atomization and Spray Systems,* pp. 205–209, Dearborn, MI, May 2001.

Received 27 February 2001; revised 25 September 2001; accepted 21 November 2001

APPENDIX

TABLE A1

Uncertainty Budget for the Fuel Flow Rate (3.0 kg hr^{-1})

	Standard uncertainty (kg hr^{-1})	
Source of uncertainty	Type A	Type B
Fuel flow/turbine frequency calibration		0.0042
Turbine meter/DAQ signal		0.0020
Repeated observations	0.015	
Combined standard uncertainty: 0.0157 kg hr^{-1}		

TABLE A2

Uncertainty Budget for the Combustion Air Flow Rate (56.7 m^3 hr^{-1})

	Standard uncertainty (m^3 hr^{-1})	
Source of uncertainty	Type A	Type B
Flow rate/pressure calibration reported by manufacturer		1.70
Pressure/voltage calibration		0.252
Comparison with calibrated pressure gauge		0.170
Repeated observations	0.024	
Combined standard uncertainty: 1.73 m^3 hr^{-1}		

TABLE A3

Inlet Conditions (z = 1.4 mm) for the Combustion Air in the Absence of the Spray Flame

Radius (mm)	Radial velocity (m/s)	Uncertainty (m/s)	Axial velocity (m/s)	Uncertainty (m/s)	Tangential velocity (m/s)	Uncertainty (m/s)	Velocity magnitude (m/s)	Uncertainty (m/s)
19.6	0.13	0.08	1.20	0.18	1.32	0.17	1.79	0.26
20.4	0.13	0.07	1.38	0.15	1.53	0.14	2.06	0.22
21.3	0.14	0.08	1.53	0.12	1.73	0.12	2.31	0.19
22.1	0.16	0.08	1.68	0.09	1.90	0.11	2.54	0.16
23.0	0.18	0.07	1.81	0.08	2.02	0.10	2.72	0.14
23.8	0.22	0.06	1.92	0.07	2.15	0.09	2.89	0.13
24.7	0.25	0.06	2.03	0.09	2.24	0.09	3.03	0.14
25.5	0.28	0.05	2.14	0.11	2.32	0.10	3.17	0.16
26.3	0.31	0.05	2.22	0.13	2.40	0.10	3.29	0.17
27.2	0.34	0.05	2.31	0.13	2.47	0.07	3.39	0.16
28.0	0.37	0.05	2.39	0.13	2.52	0.03	3.49	0.14
28.9	0.39	0.05	2.48	0.11	2.54	0.01	3.57	0.13
29.7	0.40	0.05	2.58	0.11	2.54	0.01	3.64	0.13
30.6	0.42	0.05	2.67	0.11	2.55	0.01	3.71	0.12
31.4	0.43	0.05	2.75	0.10	2.56	0.02	3.78	0.12
32.3	0.42	0.05	2.81	0.09	2.55	0.04	3.82	0.11
33.1	0.41	0.04	2.84	0.08	2.53	0.04	3.83	0.09
34.0	0.41	0.04	2.87	0.06	2.52	0.05	3.84	0.09
34.8	0.40	0.04	2.90	0.05	2.48	0.03	3.84	0.07
35.7	0.39	0.04	2.92	0.06	2.45	0.04	3.83	0.08
36.5	0.40	0.04	2.94	0.06	2.42	0.06	3.82	0.09
37.3	0.40	0.04	2.96	0.05	2.39	0.06	3.82	0.09
38.2	0.38	0.04	2.99	0.05	2.34	0.05	3.81	0.08
39.0	0.36	0.04	3.01	0.07	2.28	0.03	3.79	0.08
39.9	0.35	0.03	3.02	0.06	2.25	0.03	3.78	0.07
40.7	0.34	0.03	3.01	0.05	2.23	0.03	3.76	0.06
41.6	0.32	0.03	2.99	0.04	2.19	0.03	3.72	0.06
42.4	0.32	0.03	2.96	0.03	2.17	0.03	3.69	0.05
43.3	0.30	0.04	2.94	0.03	2.15	0.03	3.65	0.06
44.1	0.30	0.03	2.91	0.04	2.12	0.03	3.61	0.05
45.0	0.30	0.02	2.87	0.04	2.09	0.05	3.56	0.07
45.8	0.30	0.02	2.79	0.07	2.03	0.10	3.46	0.13
46.7	0.32	0.02	2.61	0.15	1.87	0.20	3.23	0.25
47.5	0.31	0.02	2.19	0.26	1.54	0.26	2.70	0.37
48.3	0.21	0.01	1.46	0.29	1.05	0.24	1.81	0.38
49.2	0.07	0.03	0.82	0.27	0.66	0.22	1.05	0.35
50.0	0.01	0.04	0.59	0.24	0.52	0.21	0.79	0.31
19.6	0.65	0.06	1.39	0.10	0.76	0.09	0.96	0.12
20.4	0.64	0.06	1.46	0.09	0.82	0.04	0.87	0.07
21.3	0.63	0.04	1.50	0.08	0.84	0.02	0.79	0.05
22.1	0.61	0.04	1.49	0.08	0.83	0.04	0.71	0.04
23.0	0.58	0.04	1.46	0.09	0.83	0.05	0.65	0.04
23.8	0.56	0.05	1.41	0.08	0.80	0.05	0.59	0.04
24.7	0.57	0.06	1.33	0.07	0.78	0.03	0.54	0.03
25.5	0.59	0.04	1.25	0.06	0.74	0.03	0.50	0.03
26.3	0.59	0.03	1.20	0.08	0.70	0.03	0.46	0.03
27.2	0.59	0.04	1.14	0.10	0.66	0.04	0.43	0.03
28.0	0.61	0.06	1.08	0.11	0.62	0.04	0.40	0.04
28.9	0.64	0.07	1.02	0.11	0.61	0.04	0.38	0.04
29.7	0.66	0.06	0.93	0.09	0.55	0.05	0.35	0.03
30.6	0.65	0.06	0.82	0.06	0.51	0.04	0.32	0.03
31.4	0.66	0.05	0.74	0.06	0.49	0.04	0.29	0.02
32.3	0.64	0.03	0.67	0.06	0.48	0.03	0.27	0.02

TABLE A3

(Continued)

Radius (mm)	Radial velocity (m/s)	Uncertainty (m/s)	Axial velocity (m/s)	Uncertainty (m/s)	Tangential velocity (m/s)	Uncertainty (m/s)	Velocity magnitude (m/s)	Uncertainty (m/s)
33.1	0.61	0.04	0.62	0.08	0.44	0.04	0.26	0.02
34.0	0.59	0.05	0.58	0.07	0.45	0.05	0.24	0.03
34.8	0.58	0.06	0.55	0.05	0.45	0.03	0.24	0.02
35.7	0.57	0.06	0.52	0.05	0.46	0.04	0.24	0.02
36.5	0.56	0.05	0.50	0.04	0.44	0.03	0.23	0.02
37.3	0.57	0.04	0.49	0.03	0.43	0.03	0.23	0.02
38.2	0.57	0.04	0.49	0.02	0.42	0.05	0.23	0.02
39.0	0.57	0.03	0.51	0.02	0.42	0.03	0.23	0.01
39.9	0.58	0.02	0.50	0.03	0.41	0.03	0.23	0.01
40.7	0.56	0.02	0.49	0.04	0.39	0.03	0.22	0.01
41.6	0.54	0.02	0.48	0.04	0.38	0.03	0.22	0.02
42.4	0.53	0.03	0.46	0.04	0.39	0.02	0.22	0.02
43.3	0.50	0.03	0.46	0.05	0.40	0.03	0.22	0.02
44.1	0.45	0.03	0.45	0.04	0.39	0.02	0.21	0.01
45.0	0.42	0.03	0.46	0.02	0.42	0.02	0.21	0.01
45.8	0.38	0.04	0.50	0.04	0.46	0.05	0.23	0.02
46.7	0.34	0.03	0.56	0.05	0.50	0.04	0.26	0.02
47.5	0.30	0.03	0.62	0.03	0.54	0.05	0.32	0.03
48.3	0.26	0.02	0.62	0.04	0.52	0.09	0.47	0.08
49.2	0.22	0.01	0.56	0.08	0.50	0.11	0.74	0.27
50.0	0.19	0.02	0.51	0.11	0.53	0.12	0.96	0.53

TABLE A4

Inlet Conditions (z = 1.4 mm) for the Combustion Air When the Spray Flame is Present

Radius (mm)	Radial velocity (m/s)	Unceratinty (m/s)	Axial velocity (m/s)	Uncertainty (m/s)	Tangential velocity (m/s)	Uncertainty (m/s)	Velocity magnitude (m/s)	Uncertainty (m/s)
19.6	0.15	0.05	1.56	0.30	1.26	0.29	2.01	0.42
20.4	0.21	0.05	1.75	0.26	1.46	0.23	2.29	0.36
21.3	0.23	0.05	1.95	0.23	1.71	0.21	2.61	0.31
22.1	0.24	0.04	2.15	0.23	2.00	0.27	2.95	0.36
23.0	0.23	0.04	2.35	0.25	2.35	0.32	3.34	0.41
23.8	0.23	0.04	2.54	0.20	2.64	0.29	3.67	0.36
24.7	0.22	0.05	2.69	0.14	2.83	0.21	3.91	0.25
25.5	0.21	0.03	2.75	0.12	2.87	0.20	3.98	0.23
26.3	0.21	0.02	2.79	0.10	2.88	0.20	4.01	0.23
27.2	0.21	0.03	2.81	0.10	2.88	0.17	4.03	0.20
28.0	0.22	0.03	2.79	0.13	2.84	0.19	3.99	0.23
28.9	0.23	0.05	2.76	0.14	2.78	0.18	3.92	0.23
29.7	0.21	0.03	2.76	0.13	2.75	0.17	3.90	0.21
30.6	0.20	0.03	2.77	0.11	2.72	0.13	3.89	0.17
31.4	0.19	0.02	2.75	0.12	2.66	0.12	3.83	0.17
32.3	0.19	0.02	2.74	0.16	2.60	0.14	3.78	0.21
33.1	0.20	0.04	2.73	0.20	2.53	0.18	3.73	0.27
34.0	0.21	0.04	2.70	0.24	2.42	0.25	3.63	0.35
34.8	0.21	0.05	2.71	0.25	2.37	0.26	3.61	0.36
35.7	0.22	0.05	2.76	0.19	2.37	0.19	3.64	0.27
36.5	0.21	0.05	2.80	0.13	2.35	0.13	3.66	0.19
37.3	0.21	0.05	2.83	0.10	2.33	0.08	3.68	0.14
38.2	0.22	0.05	2.83	0.11	2.30	0.08	3.65	0.15
39.0	0.22	0.05	2.82	0.13	2.25	0.09	3.61	0.16
39.9	0.22	0.06	2.80	0.15	2.22	0.09	3.59	0.18
40.7	0.22	0.04	2.77	0.17	2.17	0.11	3.53	0.21
41.6	0.22	0.04	2.75	0.18	2.12	0.11	3.48	0.22
42.4	0.20	0.03	2.74	0.18	2.07	0.13	3.44	0.22
43.3	0.20	0.05	2.71	0.16	2.02	0.14	3.38	0.22
44.1	0.21	0.05	2.63	0.18	1.94	0.16	3.28	0.24
45.0	0.22	0.05	2.53	0.20	1.82	0.17	3.12	0.26
45.8	0.27	0.05	2.30	0.20	1.55	0.19	2.78	0.28
46.7	0.32	0.04	1.91	0.18	1.06	0.20	2.21	0.27
47.5	0.35	0.03	1.46	0.12	0.64	0.12	1.63	0.17
48.3	0.26	0.02	0.94	0.05	0.38	0.03	1.04	0.07
49.2	0.12	0.02	0.50	0.06	0.16	0.02	0.54	0.07
50.0	0.05	0.02	0.33	0.06	0.09	0.02	0.34	0.07
19.6	0.40	0.02	0.75	0.04	0.77	0.10	0.57	0.08
20.4	0.40	0.01	0.73	0.03	0.77	0.08	0.50	0.05
21.3	0.42	0.03	0.70	0.05	0.75	0.05	0.42	0.04
22.1	0.40	0.04	0.65	0.06	0.69	0.02	0.35	0.03
23.0	0.40	0.05	0.60	0.08	0.65	0.05	0.29	0.03
23.8	0.42	0.04	0.57	0.09	0.60	0.09	0.25	0.04
24.7	0.45	0.01	0.53	0.08	0.57	0.16	0.23	0.05
25.5	0.47	0.03	0.50	0.07	0.56	0.18	0.22	0.05
26.3	0.49	0.02	0.44	0.05	0.49	0.17	0.20	0.04
27.2	0.49	0.02	0.41	0.03	0.43	0.10	0.19	0.03
28.0	0.51	0.02	0.41	0.04	0.43	0.09	0.20	0.03
28.9	0.53	0.04	0.41	0.05	0.45	0.11	0.21	0.03
29.7	0.53	0.03	0.41	0.05	0.45	0.12	0.21	0.03
30.6	0.53	0.04	0.41	0.04	0.42	0.12	0.20	0.03
31.4	0.51	0.01	0.40	0.03	0.43	0.10	0.20	0.03
32.3	0.50	0.03	0.39	0.02	0.42	0.09	0.20	0.03

TABLE A4

(Continued)

Radius (mm)	Radial velocity (m/s)	Unceratinty (m/s)	Axial velocity (m/s)	Uncertainty (m/s)	Tangential velocity (m/s)	Uncertainty (m/s)	Velocity magnitude (m/s)	Uncertainty (m/s)
33.1	0.50	0.03	0.38	0.04	0.41	0.09	0.20	0.03
34.0	0.50	0.02	0.39	0.05	0.43	0.12	0.21	0.04
34.8	0.49	0.03	0.39	0.04	0.46	0.12	0.22	0.04
35.7	0.50	0.03	0.41	0.06	0.44	0.10	0.21	0.03
36.5	0.50	0.04	0.42	0.09	0.45	0.12	0.22	0.04
37.3	0.50	0.02	0.42	0.10	0.43	0.11	0.21	0.04
38.2	0.50	0.03	0.41	0.09	0.44	0.11	0.22	0.04
39.0	0.49	0.03	0.40	0.07	0.44	0.09	0.21	0.03
39.9	0.49	0.03	0.41	0.06	0.47	0.10	0.22	0.03
40.7	0.47	0.04	0.41	0.05	0.45	0.09	0.22	0.03
41.6	0.47	0.03	0.41	0.04	0.45	0.08	0.22	0.03
42.4	0.47	0.02	0.43	0.06	0.48	0.10	0.23	0.04
43.3	0.45	0.02	0.44	0.06	0.51	0.08	0.24	0.03
44.1	0.43	0.02	0.46	0.07	0.53	0.09	0.25	0.04
45.0	0.39	0.02	0.48	0.07	0.56	0.10	0.27	0.04
45.8	0.35	0.02	0.49	0.06	0.59	0.07	0.30	0.04
46.7	0.31	0.02	0.47	0.04	0.55	0.03	0.35	0.03
47.5	0.26	0.02	0.37	0.02	0.38	0.02	0.36	0.03
48.3	0.22	0.02	0.27	0.01	0.22	0.01	0.40	0.03
49.2	0.16	0.02	0.25	0.02	0.18	0.01	0.64	0.15
50.0	0.12	0.02	0.26	0.03	0.19	0.02	1.02	0.61

TABLE A5

Downstream Air Velocity Measurements in the Absence of the Spray Flame

Radial coordinate (mm)	Axial coordinate (mm)	Radial velocity (m/s)	Uncertainty (m/s)	Axial velocity (m/s)	Uncertainty (m/s)	Tangential velocity (m/s)	Uncertainty (m/s)	Radial velocity fluctuation (m/s)	Uncertainty (m/s)	Axial velocity fluctuation (m/s)	Uncertainty (m/s)	Tangential velocity fluctuation (m/s)	Uncertainty (m/s)
−5.8	9.5	−0.18	0.08	−0.26	0.05	0.05	0.12	1.17	0.13	0.76	0.11	1.16	0.07
−5.0	9.5	−0.16	0.09	−0.28	0.07	0.08	0.13	1.17	0.11	0.74	0.11	1.16	0.07
−4.1	9.5	−0.14	0.09	−0.29	0.08	0.09	0.11	1.14	0.12	0.73	0.11	1.17	0.04
−3.3	9.5	−0.11	0.09	−0.31	0.06	0.11	0.11	1.14	0.12	0.70	0.08	1.18	0.05
−2.4	9.5	−0.08	0.10	−0.32	0.05	0.11	0.10	1.14	0.14	0.69	0.06	1.22	0.06
−1.6	9.5	−0.05	0.10	−0.33	0.05	0.12	0.08	1.14	0.11	0.71	0.06	1.23	0.07
−0.7	9.5	−0.04	0.09	−0.31	0.04	0.13	0.09	1.14	0.11	0.70	0.06	1.23	0.08
0.1	9.5	−0.03	0.10	−0.30	0.06	0.13	0.09	1.15	0.11	0.70	0.05	1.22	0.10
1.0	9.5	0.01	0.10	−0.31	0.06	0.18	0.09	1.18	0.09	0.69	0.06	1.25	0.11
1.8	9.5	0.05	0.11	−0.30	0.05	0.23	0.10	1.18	0.10	0.68	0.07	1.22	0.09
2.7	9.5	0.08	0.13	−0.29	0.06	0.27	0.11	1.17	0.11	0.67	0.07	1.18	0.07
3.5	9.5	0.09	0.16	−0.30	0.07	0.29	0.10	1.17	0.09	0.66	0.07	1.16	0.07
4.4	9.5	0.06	0.17	−0.29	0.07	0.34	0.08	1.20	0.07	0.65	0.06	1.15	0.12
5.2	9.5	0.05	0.17	−0.26	0.07	0.40	0.09	1.19	0.06	0.65	0.05	1.12	0.12
6.0	9.5	0.04	0.16	−0.24	0.07	0.46	0.10	1.19	0.06	0.68	0.04	1.08	0.08
6.9	9.5	0.05	0.16	−0.21	0.06	0.52	0.12	1.20	0.07	0.72	0.03	1.05	0.08
7.7	9.5	0.07	0.15	−0.18	0.06	0.58	0.13	1.22	0.05	0.76	0.03	1.05	0.05
8.6	9.5	0.08	0.12	−0.13	0.07	0.67	0.12	1.22	0.05	0.79	0.03	1.02	0.05
9.4	9.5	0.08	0.10	−0.08	0.09	0.75	0.13	1.22	0.06	0.81	0.05	1.02	0.06
10.3	9.5	0.11	0.11	−0.02	0.11	0.83	0.13	1.20	0.08	0.86	0.05	1.01	0.06
11.1	9.5	0.12	0.10	0.05	0.14	0.90	0.13	1.18	0.11	0.92	0.05	1.02	0.08
12.0	9.5	0.11	0.11	0.12	0.16	0.97	0.14	1.17	0.09	0.98	0.06	1.03	0.13
12.8	9.5	0.10	0.09	0.21	0.15	1.06	0.15	1.18	0.08	1.02	0.09	1.00	0.12
13.7	9.5	0.10	0.10	0.32	0.15	1.09	0.12	1.17	0.05	1.09	0.10	0.98	0.11
14.5	9.5	0.11	0.11	0.48	0.14	1.17	0.11	1.15	0.04	1.18	0.10	0.98	0.06
15.4	9.5	0.14	0.11	0.63	0.14	1.25	0.11	1.12	0.04	1.28	0.09	1.01	0.08
16.2	9.5	0.15	0.11	0.76	0.14	1.29	0.08	1.07	0.04	1.33	0.10	0.98	0.06
17.0	9.5	0.16	0.10	0.87	0.13	1.33	0.07	1.04	0.03	1.39	0.10	0.95	0.05
17.9	9.5	0.15	0.08	0.97	0.13	1.39	0.06	0.99	0.05	1.43	0.09	0.94	0.04
18.7	9.5	0.17	0.08	1.07	0.14	1.49	0.06	0.94	0.06	1.44	0.07	0.93	0.05
19.6	9.5	0.16	0.06	1.16	0.12	1.58	0.06	0.88	0.05	1.44	0.07	0.93	0.03
20.4	9.5	0.18	0.06	1.26	0.11	1.68	0.06	0.84	0.05	1.43	0.07	0.94	0.05
21.3	9.5	0.21	0.08	1.35	0.11	1.76	0.05	0.79	0.05	1.41	0.09	0.96	0.06
22.1	9.5	0.25	0.11	1.43	0.10	1.83	0.04	0.75	0.05	1.38	0.11	0.97	0.08
23.0	9.5	0.28	0.12	1.50	0.10	1.89	0.05	0.72	0.04	1.38	0.12	0.94	0.06

TABLE A5

(Continued)

Radial coordinate (mm)	Axial coordinate (mm)	Radial velocity (m/s)	Uncertainty (m/s)	Axial velocity (m/s)	Uncertainty (m/s)	Tangential velocity (m/s)	Uncertainty (m/s)	Radial velocity fluctuation (m/s)	Uncertainty (m/s)	Axial velocity fluctuation (m/s)	Uncertainty (m/s)	Tangential velocity fluctuation (m/s)	Uncertainty (m/s)
23.8	9.5	0.30	0.12	1.57	0.11	1.95	0.04	0.71	0.02	1.38	0.13	0.90	0.05
24.7	9.5	0.33	0.12	1.65	0.13	1.99	0.04	0.70	0.02	1.37	0.12	0.86	0.06
25.5	9.5	0.35	0.12	1.76	0.14	2.04	0.05	0.68	0.04	1.34	0.10	0.85	0.09
26.3	9.5	0.35	0.11	1.87	0.16	2.09	0.06	0.66	0.03	1.27	0.09	0.82	0.08
27.2	9.5	0.36	0.10	1.98	0.16	2.14	0.06	0.65	0.03	1.21	0.08	0.80	0.10
28.0	9.5	0.38	0.09	2.09	0.14	2.17	0.06	0.65	0.05	1.19	0.06	0.75	0.07
28.9	9.5	0.42	0.10	2.20	0.12	2.24	0.04	0.65	0.07	1.16	0.08	0.72	0.03
29.7	9.5	0.45	0.10	2.32	0.11	2.27	0.06	0.65	0.07	1.13	0.09	0.68	0.06
30.6	9.5	0.45	0.11	2.43	0.11	2.31	0.09	0.64	0.06	1.09	0.11	0.66	0.10
31.4	9.5	0.46	0.11	2.52	0.12	2.33	0.10	0.65	0.06	1.02	0.13	0.64	0.09
32.3	9.5	0.47	0.09	2.59	0.14	2.34	0.13	0.68	0.06	0.93	0.12	0.60	0.08
33.1	9.5	0.47	0.08	2.67	0.15	2.34	0.12	0.67	0.06	0.87	0.11	0.58	0.07
34.0	9.5	0.47	0.09	2.76	0.12	2.34	0.10	0.66	0.05	0.80	0.07	0.57	0.07
34.8	9.5	0.49	0.07	2.83	0.07	2.35	0.08	0.63	0.05	0.74	0.05	0.52	0.03
35.7	9.5	0.50	0.05	2.89	0.05	2.34	0.05	0.60	0.06	0.70	0.04	0.49	0.07
36.5	9.5	0.51	0.04	2.94	0.04	2.34	0.04	0.60	0.06	0.67	0.04	0.45	0.07
37.3	9.5	0.53	0.05	2.97	0.03	2.34	0.06	0.59	0.07	0.64	0.03	0.44	0.07
38.2	9.5	0.51	0.04	3.00	0.03	2.29	0.07	0.61	0.08	0.61	0.04	0.43	0.04
39.0	9.5	0.50	0.04	3.02	0.03	2.27	0.06	0.61	0.09	0.59	0.03	0.44	0.03
39.9	9.5	0.50	0.03	3.04	0.04	2.25	0.05	0.61	0.10	0.58	0.03	0.41	0.04
40.7	9.5	0.48	0.04	3.04	0.04	2.21	0.06	0.60	0.09	0.57	0.04	0.41	0.04
41.6	9.5	0.47	0.04	3.04	0.04	2.17	0.05	0.60	0.08	0.53	0.05	0.41	0.03
42.4	9.5	0.48	0.04	3.03	0.04	2.16	0.05	0.57	0.08	0.50	0.06	0.43	0.01
43.3	9.5	0.47	0.04	3.01	0.04	2.15	0.03	0.54	0.09	0.49	0.03	0.42	0.02
44.1	9.5	0.47	0.05	2.99	0.04	2.13	0.05	0.52	0.08	0.49	0.01	0.41	0.03
45.0	9.5	0.47	0.06	2.96	0.05	2.11	0.06	0.49	0.08	0.52	0.04	0.41	0.02
45.8	9.5	0.47	0.05	2.92	0.05	2.08	0.04	0.47	0.08	0.53	0.06	0.42	0.01
46.7	9.5	0.48	0.05	2.86	0.04	2.07	0.03	0.47	0.09	0.54	0.06	0.40	0.03
47.5	9.5	0.47	0.05	2.75	0.03	2.00	0.05	0.48	0.06	0.56	0.05	0.42	0.05
48.3	9.5	0.45	0.06	2.51	0.04	1.87	0.08	0.51	0.06	0.59	0.06	0.44	0.09
49.2	9.5	0.38	0.06	2.18	0.06	1.63	0.09	0.55	0.07	0.64	0.09	0.51	0.08
50.0	9.5	0.28	0.05	1.93	0.07	1.36	0.07	0.54	0.06	0.69	0.08	0.55	0.05
−5.8	17.6	0.01	0.12	−0.37	0.04	−0.02	0.14	1.09	0.10	0.87	0.10	1.09	0.07
−5.0	17.6	0.00	0.12	−0.37	0.02	0.04	0.14	1.08	0.08	0.87	0.10	1.10	0.07
−4.1	17.6	0.00	0.11	−0.37	0.02	0.11	0.14	1.08	0.07	0.87	0.10	1.08	0.06

TABLE A5

(Continued)

Radial coordinate (mm)	Axial coordinate (mm)	Radial velocity (m/s)	Uncertainty (m/s)	Axial velocity (m/s)	Uncertainty (m/s)	Tangential velocity (m/s)	Uncertainty (m/s)	Radial velocity fluctuation (m/s)	Uncertainty (m/s)	Axial velocity fluctuation (m/s)	Uncertainty (m/s)	Tangential velocity fluctuation (m/s)	Uncertainty (m/s)
−3.3	17.6	0.03	0.10	−0.37	0.04	0.15	0.14	1.08	0.05	0.85	0.08	1.08	0.05
−2.4	17.6	0.06	0.10	−0.38	0.08	0.20	0.12	1.09	0.07	0.83	0.09	1.09	0.03
−1.6	17.6	0.05	0.10	−0.39	0.12	0.22	0.08	1.09	0.07	0.83	0.09	1.08	0.04
−0.7	17.6	0.07	0.09	−0.40	0.13	0.29	0.08	1.08	0.08	0.83	0.08	1.10	0.09
0.1	17.6	0.07	0.09	−0.40	0.13	0.32	0.09	1.07	0.08	0.82	0.07	1.10	0.11
1.0	17.6	0.07	0.08	−0.40	0.12	0.36	0.10	1.07	0.07	0.82	0.06	1.12	0.12
1.8	17.6	0.07	0.07	−0.41	0.13	0.42	0.09	1.08	0.07	0.82	0.06	1.12	0.13
2.7	17.6	0.06	0.07	−0.40	0.13	0.49	0.07	1.08	0.07	0.83	0.06	1.12	0.12
3.5	17.6	0.07	0.10	−0.40	0.13	0.58	0.07	1.04	0.09	0.85	0.05	1.12	0.13
4.4	17.6	0.08	0.11	−0.37	0.12	0.65	0.08	1.00	0.10	0.87	0.04	1.10	0.15
5.2	17.6	0.08	0.11	−0.35	0.11	0.71	0.09	1.01	0.09	0.88	0.03	1.11	0.15
6.0	17.6	0.07	0.11	−0.32	0.11	0.75	0.09	1.01	0.09	0.89	0.02	1.08	0.15
6.9	17.6	0.08	0.10	−0.28	0.13	0.81	0.08	1.03	0.08	0.91	0.04	1.06	0.14
7.7	17.6	0.07	0.08	−0.23	0.13	0.85	0.08	1.03	0.07	0.93	0.06	1.04	0.14
8.6	17.6	0.07	0.08	−0.20	0.14	0.89	0.09	1.05	0.09	0.96	0.04	1.02	0.12
9.4	17.6	0.07	0.07	−0.14	0.14	0.94	0.11	1.04	0.08	1.00	0.03	1.06	0.13
10.3	17.6	0.06	0.08	−0.06	0.14	0.99	0.12	1.02	0.09	1.05	0.03	1.09	0.15
11.1	17.6	0.04	0.09	0.03	0.14	1.02	0.11	1.00	0.10	1.08	0.03	1.04	0.13
12.0	17.6	0.05	0.10	0.15	0.12	1.10	0.10	1.00	0.10	1.13	0.02	0.98	0.10
12.8	17.6	0.05	0.10	0.24	0.11	1.14	0.10	0.98	0.11	1.16	0.04	0.98	0.09
13.7	17.6	0.06	0.08	0.31	0.13	1.19	0.09	0.94	0.11	1.20	0.07	0.97	0.10
14.5	17.6	0.07	0.08	0.39	0.13	1.26	0.06	0.91	0.11	1.22	0.08	0.95	0.14
15.4	17.6	0.09	0.09	0.46	0.14	1.30	0.05	0.86	0.10	1.25	0.08	0.96	0.12
16.2	17.6	0.10	0.07	0.54	0.13	1.35	0.05	0.83	0.11	1.29	0.06	0.94	0.06
17.0	17.6	0.12	0.08	0.63	0.12	1.41	0.04	0.82	0.12	1.34	0.03	0.92	0.05
17.9	17.6	0.14	0.07	0.72	0.11	1.48	0.04	0.80	0.11	1.38	0.04	0.91	0.07
18.7	17.6	0.15	0.07	0.82	0.09	1.52	0.05	0.77	0.11	1.40	0.07	0.91	0.09
19.6	17.6	0.18	0.06	0.92	0.08	1.56	0.04	0.74	0.09	1.40	0.08	0.90	0.10
20.4	17.6	0.21	0.06	1.01	0.09	1.59	0.05	0.72	0.08	1.37	0.07	0.90	0.10
21.3	17.6	0.23	0.05	1.08	0.10	1.63	0.08	0.72	0.09	1.34	0.07	0.88	0.09
22.1	17.6	0.25	0.07	1.15	0.10	1.66	0.07	0.70	0.11	1.33	0.07	0.85	0.08
23.0	17.6	0.27	0.09	1.24	0.09	1.70	0.08	0.68	0.08	1.32	0.05	0.86	0.05
23.8	17.6	0.26	0.09	1.33	0.09	1.70	0.09	0.67	0.06	1.31	0.04	0.85	0.05
24.7	17.6	0.28	0.09	1.41	0.09	1.76	0.09	0.65	0.05	1.30	0.04	0.83	0.04
25.5	17.6	0.32	0.06	1.50	0.10	1.83	0.08	0.65	0.04	1.31	0.04	0.81	0.03

TABLE A5

(Continued)

Radial coordinate (mm)	Axial coordinate (mm)	Radial velocity (m/s)	Uncertainty (m/s)	Axial velocity (m/s)	Uncertainty (m/s)	Tangential velocity (m/s)	Uncertainty (m/s)	Radial velocity fluctuation (m/s)	Uncertainty (m/s)	Axial velocity fluctuation (m/s)	Uncertainty (m/s)	Tangential velocity fluctuation (m/s)	Uncertainty (m/s)
26.3	17.6	0.33	0.04	1.59	0.11	1.87	0.07	0.66	0.06	1.30	0.05	0.78	0.04
27.2	17.6	0.37	0.05	1.67	0.11	1.92	0.06	0.67	0.05	1.27	0.06	0.77	0.03
28.0	17.6	0.40	0.08	1.78	0.10	1.98	0.06	0.67	0.05	1.25	0.07	0.75	0.02
28.9	17.6	0.43	0.06	1.90	0.08	2.01	0.07	0.67	0.04	1.24	0.06	0.73	0.03
29.7	17.6	0.45	0.07	2.02	0.08	2.05	0.06	0.64	0.02	1.22	0.05	0.71	0.03
30.6	17.6	0.46	0.08	2.14	0.09	2.08	0.06	0.63	0.02	1.20	0.05	0.69	0.03
31.4	17.6	0.48	0.11	2.24	0.10	2.09	0.06	0.61	0.02	1.17	0.06	0.68	0.05
32.3	17.6	0.51	0.11	2.33	0.13	2.12	0.04	0.63	0.03	1.14	0.07	0.63	0.05
33.1	17.6	0.52	0.09	2.42	0.14	2.14	0.05	0.63	0.04	1.10	0.10	0.62	0.04
34.0	17.6	0.53	0.08	2.51	0.14	2.15	0.06	0.63	0.05	1.05	0.10	0.63	0.04
34.8	17.6	0.55	0.07	2.60	0.14	2.15	0.08	0.64	0.04	0.98	0.08	0.62	0.06
35.7	17.6	0.57	0.07	2.68	0.15	2.16	0.09	0.66	0.03	0.93	0.08	0.60	0.06
36.5	17.6	0.58	0.05	2.76	0.14	2.17	0.09	0.65	0.03	0.87	0.06	0.56	0.05
37.3	17.6	0.60	0.05	2.81	0.13	2.19	0.10	0.64	0.03	0.85	0.06	0.56	0.05
38.2	17.6	0.62	0.06	2.86	0.11	2.22	0.08	0.64	0.03	0.85	0.08	0.57	0.06
39.0	17.6	0.62	0.06	2.92	0.08	2.21	0.05	0.63	0.03	0.80	0.07	0.53	0.05
39.9	17.6	0.63	0.06	2.96	0.06	2.21	0.04	0.63	0.06	0.76	0.08	0.48	0.05
40.7	17.6	0.63	0.06	2.99	0.07	2.21	0.04	0.62	0.06	0.73	0.06	0.47	0.04
41.6	17.6	0.64	0.06	3.02	0.07	2.19	0.04	0.61	0.05	0.68	0.04	0.47	0.03
42.4	17.6	0.62	0.05	3.03	0.06	2.17	0.04	0.59	0.04	0.64	0.04	0.45	0.02
43.3	17.6	0.60	0.05	3.02	0.05	2.16	0.05	0.60	0.04	0.63	0.05	0.45	0.04
44.1	17.6	0.59	0.05	3.03	0.03	2.13	0.04	0.58	0.04	0.60	0.03	0.43	0.02
45.0	17.6	0.58	0.05	3.02	0.04	2.10	0.04	0.56	0.03	0.59	0.02	0.42	0.02
45.8	17.6	0.56	0.05	2.99	0.04	2.08	0.05	0.57	0.03	0.59	0.05	0.43	0.04
46.7	17.6	0.56	0.07	2.93	0.01	2.05	0.05	0.56	0.04	0.57	0.06	0.46	0.04
47.5	17.6	0.56	0.07	2.84	0.04	1.96	0.08	0.56	0.06	0.58	0.06	0.51	0.12
48.3	17.6	0.54	0.07	2.70	0.06	1.82	0.12	0.59	0.04	0.60	0.05	0.62	0.26
49.2	17.6	0.49	0.08	2.54	0.09	1.63	0.19	0.64	0.04	0.67	0.06	0.80	0.46
50.0	17.6	0.39	0.09	2.39	0.12	1.40	0.20	0.63	0.06	0.73	0.09	0.89	0.57

TABLE A6

Downstream Air Velocity Measurements When the Spray Flame is Present

Radial coordinate (mm)	Axial coordinate (mm)	Radial velocity (m/s)	Uncertainty (m/s)	Axial velocity (m/s)	Uncertainty (m/s)	Tangential velocity (m/s)	Uncertainty (m/s)	Radial velocity fluctuation (m/s)	Uncertainty (m/s)	Axial velocity fluctuation (m/s)	Uncertainty (m/s)	Tangential velocity fluctuation (m/s)	Uncertainty (m/s)
−5.8	9.5	0.17	0.12	0.21	0.24	0.05	0.37	3.26	0.27	2.28	0.34	3.86	0.30
−5.0	9.5	0.21	0.15	0.16	0.24	0.02	0.31	3.09	0.31	2.24	0.29	3.79	0.32
−4.1	9.5	0.24	0.18	0.13	0.23	0.09	0.32	2.95	0.36	2.24	0.24	3.86	0.33
−3.3	9.5	0.23	0.16	0.13	0.24	0.07	0.27	2.82	0.41	2.26	0.23	3.95	0.35
−2.4	9.5	0.14	0.20	0.11	0.21	0.09	0.21	2.67	0.39	2.29	0.20	3.92	0.34
−1.6	9.5	0.07	0.21	0.10	0.19	0.17	0.25	2.43	0.29	2.31	0.17	3.80	0.22
−0.7	9.5	0.07	0.19	0.10	0.20	0.35	0.22	2.24	0.20	2.34	0.18	3.64	0.21
0.1	9.5	0.04	0.16	0.03	0.20	0.58	0.22	2.17	0.24	2.37	0.17	3.51	0.32
1.0	9.5	−0.06	0.16	−0.03	0.20	0.74	0.22	2.16	0.33	2.31	0.18	3.41	0.52
1.8	9.5	−0.23	0.18	−0.06	0.26	0.96	0.21	2.05	0.38	2.21	0.22	3.12	0.60
2.7	9.5	−0.37	0.22	−0.04	0.24	1.14	0.26	2.02	0.46	2.03	0.30	2.88	0.71
3.5	9.5	−0.54	0.29	−0.01	0.19	1.33	0.30	1.88	0.49	1.81	0.34	2.60	0.66
4.4	9.5	−0.73	0.31	−0.03	0.13	1.53	0.37	1.62	0.51	1.45	0.34	2.24	0.60
5.2	9.5	−0.84	0.29	−0.08	0.09	1.73	0.36	1.21	0.37	1.07	0.31	1.77	0.51
6.0	9.5	−0.80	0.30	−0.13	0.10	1.92	0.31	0.98	0.33	0.93	0.30	1.41	0.53
6.9	9.5	−0.73	0.25	−0.15	0.09	2.01	0.21	0.87	0.36	0.87	0.27	1.25	0.47
7.7	9.5	−0.63	0.17	−0.17	0.11	2.06	0.14	0.76	0.28	0.77	0.21	1.07	0.37
8.6	9.5	−0.51	0.10	−0.16	0.11	2.08	0.14	0.59	0.13	0.67	0.15	0.92	0.24
9.4	9.5	−0.42	0.07	−0.10	0.09	2.08	0.11	0.54	0.04	0.62	0.10	0.83	0.16
10.3	9.5	−0.34	0.05	−0.03	0.09	2.08	0.06	0.53	0.04	0.62	0.04	0.76	0.12
11.1	9.5	−0.28	0.05	0.08	0.08	2.06	0.04	0.52	0.04	0.64	0.03	0.71	0.11
12.0	9.5	−0.23	0.06	0.19	0.06	2.01	0.03	0.51	0.05	0.67	0.02	0.74	0.13
12.8	9.5	−0.21	0.06	0.35	0.04	2.02	0.02	0.52	0.03	0.73	0.02	0.71	0.10
13.7	9.5	−0.19	0.05	0.55	0.04	2.05	0.02	0.53	0.03	0.79	0.03	0.69	0.05
14.5	9.5	−0.20	0.05	0.76	0.02	2.06	0.03	0.52	0.05	0.85	0.05	0.69	0.05
15.4	9.5	−0.20	0.04	0.99	0.05	2.08	0.06	0.52	0.07	0.89	0.07	0.69	0.05
16.2	9.5	−0.20	0.04	1.22	0.07	2.13	0.06	0.49	0.05	0.93	0.06	0.64	0.06
17.0	9.5	−0.16	0.06	1.47	0.07	2.21	0.06	0.47	0.04	0.93	0.05	0.66	0.07
17.9	9.5	−0.12	0.06	1.71	0.07	2.32	0.05	0.48	0.04	0.92	0.04	0.67	0.06
18.7	9.5	−0.08	0.05	1.91	0.07	2.42	0.04	0.47	0.03	0.89	0.02	0.66	0.06
19.6	9.5	−0.04	0.03	2.08	0.07	2.52	0.04	0.43	0.02	0.86	0.02	0.62	0.05
20.4	9.5	0.01	0.04	2.23	0.05	2.61	0.04	0.42	0.02	0.81	0.04	0.59	0.03
21.3	9.5	0.05	0.04	2.39	0.04	2.70	0.05	0.42	0.01	0.77	0.05	0.55	0.02
22.1	9.5	0.09	0.05	2.50	0.04	2.79	0.06	0.43	0.01	0.73	0.07	0.51	0.04
23.0	9.5	0.13	0.04	2.59	0.06	2.85	0.05	0.42	0.02	0.67	0.07	0.48	0.06

TABLE A6

(Continued)

Radial coordinate (mm)	Axial coordinate (mm)	Radial velocity (m/s)	Uncertainty (m/s)	Axial velocity (m/s)	Uncertainty (m/s)	Tangential velocity (m/s)	Uncertainty (m/s)	Radial velocity fluctuation (m/s)	Uncertainty (m/s)	Axial velocity fluctuation (m/s)	Uncertainty (m/s)	Tangential velocity fluctuation (m/s)	Uncertainty (m/s)
23.8	9.5	0.17	0.05	2.66	0.06	2.91	0.05	0.42	0.04	0.61	0.07	0.45	0.02
24.7	9.5	0.20	0.06	2.73	0.06	2.92	0.05	0.43	0.04	0.57	0.06	0.44	0.02
25.5	9.5	0.22	0.04	2.76	0.08	2.92	0.05	0.45	0.04	0.54	0.06	0.44	0.05
26.3	9.5	0.24	0.04	2.79	0.07	2.92	0.05	0.45	0.04	0.50	0.04	0.44	0.05
27.2	9.5	0.27	0.05	2.81	0.07	2.93	0.04	0.46	0.03	0.47	0.03	0.41	0.02
28.0	9.5	0.28	0.07	2.83	0.06	2.89	0.05	0.46	0.03	0.45	0.02	0.39	0.02
28.9	9.5	0.29	0.07	2.85	0.03	2.85	0.06	0.48	0.04	0.42	0.01	0.37	0.01
29.7	9.5	0.30	0.08	2.86	0.02	2.80	0.06	0.48	0.04	0.41	0.01	0.36	0.01
30.6	9.5	0.29	0.08	2.86	0.01	2.76	0.06	0.49	0.05	0.40	0.02	0.36	0.02
31.4	9.5	0.29	0.08	2.87	0.02	2.73	0.05	0.49	0.05	0.39	0.02	0.37	0.05
32.3	9.5	0.29	0.09	2.87	0.02	2.68	0.05	0.49	0.03	0.38	0.02	0.37	0.03
33.1	9.5	0.30	0.10	2.87	0.02	2.64	0.06	0.49	0.04	0.37	0.01	0.36	0.03
34.0	9.5	0.29	0.09	2.89	0.01	2.59	0.05	0.50	0.02	0.38	0.01	0.34	0.01
34.8	9.5	0.30	0.08	2.90	0.01	2.54	0.05	0.50	0.02	0.37	0.01	0.34	0.03
35.7	9.5	0.30	0.09	2.91	0.02	2.50	0.05	0.51	0.02	0.37	0.01	0.35	0.03
36.5	9.5	0.30	0.07	2.92	0.03	2.45	0.05	0.52	0.02	0.37	0.03	0.35	0.00
37.3	9.5	0.30	0.07	2.93	0.04	2.43	0.06	0.51	0.02	0.37	0.02	0.35	0.03
38.2	9.5	0.30	0.07	2.93	0.06	2.39	0.05	0.50	0.03	0.36	0.02	0.37	0.01
39.0	9.5	0.29	0.06	2.93	0.06	2.34	0.04	0.52	0.03	0.36	0.02	0.38	0.03
39.9	9.5	0.28	0.05	2.92	0.06	2.29	0.03	0.51	0.03	0.36	0.03	0.37	0.03
40.7	9.5	0.27	0.05	2.92	0.05	2.27	0.03	0.50	0.03	0.36	0.02	0.36	0.02
41.6	9.5	0.26	0.05	2.93	0.05	2.23	0.02	0.50	0.02	0.38	0.02	0.37	0.01
42.4	9.5	0.26	0.05	2.93	0.05	2.20	0.05	0.49	0.02	0.39	0.03	0.40	0.02
43.3	9.5	0.25	0.05	2.91	0.04	2.17	0.03	0.46	0.01	0.40	0.03	0.43	0.03
44.1	9.5	0.25	0.04	2.85	0.03	2.10	0.02	0.43	0.01	0.42	0.02	0.44	0.02
45.0	9.5	0.25	0.04	2.78	0.04	2.03	0.05	0.41	0.01	0.42	0.01	0.49	0.04
45.8	9.5	0.26	0.04	2.67	0.05	1.92	0.07	0.39	0.03	0.44	0.01	0.54	0.04
46.6	9.5	0.29	0.05	2.49	0.06	1.73	0.10	0.38	0.03	0.46	0.00	0.60	0.03
47.5	9.5	0.31	0.06	2.23	0.06	1.46	0.08	0.37	0.02	0.50	0.01	0.61	0.04
48.3	9.5	0.31	0.06	1.94	0.04	1.25	0.07	0.40	0.02	0.52	0.02	0.62	0.07
49.2	9.5	0.28	0.06	1.64	0.02	1.06	0.07	0.44	0.03	0.55	0.04	0.63	0.09
50.0	9.5	0.14	0.11	1.46	0.05	0.92	0.15	0.39	0.07	0.60	0.07	0.67	0.09
−5.8	17.6	0.39	0.43	0.72	0.69	0.64	0.56	5.03	0.97	3.66	0.42	5.61	0.46
−5.0	17.6	0.40	0.42	0.66	0.72	0.61	0.52	4.99	0.96	3.63	0.42	5.62	0.38
−4.1	17.6	0.38	0.45	0.61	0.73	0.48	0.50	4.93	0.98	3.58	0.48	5.75	0.48

TABLE A6

(Continued)

Radial coordinate (mm)	Axial coordinate (mm)	Radial velocity (m/s)	Uncertainty (m/s)	Axial velocity (m/s)	Uncertainty (m/s)	Tangential velocity (m/s)	Uncertainty (m/s)	Radial velocity fluctuation (m/s)	Uncertainty (m/s)	Axial velocity fluctuation (m/s)	Uncertainty (m/s)	Tangential velocity fluctuation (m/s)	Uncertainty (m/s)
−3.3	17.6	0.36	0.45	0.56	0.73	0.37	0.43	4.89	1.02	3.53	0.54	5.90	0.59
−2.4	17.6	0.39	0.45	0.57	0.76	0.28	0.37	4.77	1.09	3.58	0.60	6.00	0.66
−1.6	17.6	0.38	0.42	0.54	0.85	0.25	0.34	4.54	1.05	3.59	0.63	5.96	0.67
−0.7	17.6	0.44	0.39	0.60	0.94	0.31	0.29	4.44	0.94	3.59	0.65	5.99	0.68
0.1	17.6	0.56	0.37	0.67	1.03	0.40	0.23	4.40	0.85	3.55	0.61	5.91	0.73
1.0	17.6	0.64	0.34	0.76	1.09	0.50	0.15	4.20	0.67	3.52	0.52	5.75	0.70
1.8	17.6	0.65	0.32	0.81	1.15	0.62	0.10	4.06	0.62	3.49	0.45	5.67	0.76
2.7	17.6	0.60	0.38	0.81	1.20	0.67	0.17	4.03	0.68	3.52	0.44	5.60	0.87
3.5	17.6	0.54	0.42	0.82	1.24	0.75	0.32	4.03	0.73	3.55	0.50	5.51	0.85
4.4	17.6	0.55	0.40	0.83	1.24	0.92	0.45	4.08	0.76	3.55	0.56	5.36	0.77
5.2	17.6	0.52	0.40	0.86	1.14	1.10	0.37	4.06	0.74	3.43	0.56	5.12	0.71
6.0	17.6	0.46	0.37	0.82	1.03	1.25	0.33	3.98	0.74	3.29	0.57	4.89	0.74
6.9	17.6	0.40	0.39	0.77	0.90	1.42	0.33	3.81	0.73	3.13	0.58	4.62	0.81
7.7	17.6	0.26	0.41	0.71	0.77	1.53	0.39	3.63	0.79	2.91	0.64	4.19	0.90
8.6	17.6	0.04	0.30	0.60	0.58	1.56	0.32	3.20	0.81	2.57	0.67	3.55	0.94
9.4	17.6	−0.14	0.16	0.48	0.34	1.64	0.21	2.70	0.80	2.19	0.60	2.99	0.89
10.3	17.6	−0.23	0.11	0.35	0.18	1.79	0.10	2.12	0.56	1.76	0.41	2.37	0.65
11.1	17.6	−0.32	0.04	0.24	0.10	1.88	0.10	1.52	0.25	1.37	0.26	1.87	0.48
12.0	17.6	−0.39	0.07	0.20	0.12	1.89	0.14	1.09	0.22	1.16	0.18	1.60	0.46
12.8	17.6	−0.38	0.12	0.21	0.10	1.92	0.15	0.88	0.26	1.04	0.13	1.35	0.46
13.7	17.6	−0.33	0.15	0.35	0.11	1.95	0.10	0.77	0.22	1.01	0.10	1.12	0.33
14.5	17.6	−0.28	0.14	0.52	0.12	1.93	0.08	0.67	0.16	0.99	0.06	0.95	0.21
15.4	17.6	−0.24	0.10	0.68	0.09	1.98	0.05	0.59	0.13	0.95	0.03	0.84	0.16
16.2	17.6	−0.18	0.09	0.85	0.09	2.10	0.02	0.54	0.10	0.94	0.02	0.78	0.15
17.0	17.6	−0.10	0.09	1.04	0.06	2.21	0.06	0.49	0.06	0.94	0.04	0.72	0.12
17.9	17.6	−0.05	0.08	1.22	0.04	2.26	0.06	0.50	0.06	0.96	0.05	0.70	0.12
18.7	17.6	−0.01	0.08	1.40	0.02	2.31	0.09	0.48	0.04	0.97	0.06	0.67	0.09
19.6	17.6	0.04	0.08	1.58	0.01	2.37	0.08	0.45	0.01	0.96	0.09	0.64	0.07
20.4	17.6	0.08	0.08	1.75	0.01	2.42	0.07	0.47	0.01	0.93	0.06	0.65	0.10
21.3	17.6	0.11	0.09	1.92	0.04	2.47	0.05	0.49	0.03	0.89	0.04	0.62	0.09
22.1	17.6	0.17	0.07	2.07	0.05	2.53	0.05	0.47	0.03	0.82	0.03	0.59	0.03
23.0	17.6	0.19	0.06	2.20	0.06	2.59	0.05	0.47	0.02	0.77	0.01	0.57	0.02
23.8	17.6	0.23	0.05	2.31	0.07	2.65	0.06	0.48	0.05	0.72	0.02	0.54	0.03
24.7	17.6	0.27	0.05	2.42	0.07	2.70	0.07	0.49	0.06	0.67	0.04	0.53	0.04
25.5	17.6	0.29	0.07	2.50	0.07	2.73	0.09	0.48	0.03	0.61	0.04	0.49	0.03

TABLE A6

(Continued)

Radial coordinate (mm)	Axial coordinate (mm)	Radial velocity (m/s)	Uncertainty (m/s)	Axial velocity (m/s)	Uncertainty (m/s)	Tangential velocity (m/s)	Uncertainty (m/s)	Radial velocity fluctuation (m/s)	Uncertainty (m/s)	Axial velocity fluctuation (m/s)	Uncertainty (m/s)	Tangential velocity fluctuation (m/s)	Uncertainty (m/s)
26.3	17.6	0.31	0.06	2.59	0.07	2.74	0.07	0.46	0.02	0.57	0.05	0.47	0.04
27.2	17.6	0.32	0.05	2.65	0.05	2.73	0.05	0.45	0.02	0.54	0.04	0.45	0.05
28.0	17.6	0.35	0.06	2.70	0.04	2.73	0.05	0.46	0.01	0.51	0.04	0.40	0.04
28.9	17.6	0.37	0.05	2.73	0.04	2.73	0.04	0.48	0.02	0.48	0.03	0.38	0.03
29.7	17.6	0.39	0.07	2.76	0.04	2.72	0.05	0.48	0.03	0.44	0.02	0.38	0.02
30.6	17.6	0.40	0.06	2.78	0.05	2.71	0.04	0.48	0.04	0.42	0.02	0.37	0.04
31.4	17.6	0.41	0.05	2.80	0.05	2.68	0.05	0.49	0.03	0.41	0.03	0.37	0.03
32.3	17.6	0.42	0.07	2.83	0.05	2.65	0.06	0.50	0.02	0.39	0.02	0.38	0.03
33.1	17.6	0.40	0.07	2.84	0.03	2.61	0.06	0.48	0.02	0.39	0.03	0.40	0.02
34.0	17.6	0.39	0.07	2.86	0.03	2.55	0.04	0.50	0.02	0.39	0.03	0.36	0.02
34.8	17.6	0.39	0.07	2.87	0.01	2.50	0.04	0.51	0.03	0.39	0.03	0.37	0.02
35.7	17.6	0.39	0.07	2.88	0.02	2.47	0.03	0.52	0.03	0.37	0.01	0.39	0.03
36.5	17.6	0.38	0.07	2.91	0.03	2.43	0.05	0.51	0.03	0.36	0.01	0.42	0.03
37.3	17.6	0.38	0.08	2.91	0.03	2.41	0.04	0.51	0.03	0.36	0.01	0.42	0.02
38.2	17.6	0.37	0.09	2.90	0.02	2.36	0.06	0.51	0.03	0.36	0.02	0.42	0.03
39.0	17.6	0.37	0.07	2.91	0.02	2.32	0.05	0.51	0.03	0.36	0.02	0.43	0.03
39.9	17.6	0.36	0.05	2.92	0.03	2.28	0.03	0.51	0.03	0.37	0.02	0.40	0.01
40.7	17.6	0.36	0.05	2.93	0.03	2.25	0.02	0.50	0.02	0.37	0.02	0.38	0.04
41.6	17.6	0.34	0.05	2.93	0.04	2.20	0.02	0.48	0.02	0.38	0.01	0.39	0.02
42.4	17.6	0.34	0.03	2.91	0.04	2.18	0.02	0.47	0.02	0.39	0.03	0.42	0.01
43.3	17.6	0.33	0.03	2.89	0.05	2.13	0.01	0.46	0.01	0.39	0.03	0.42	0.03
44.1	17.6	0.34	0.03	2.85	0.06	2.06	0.01	0.44	0.02	0.41	0.02	0.48	0.02
45.0	17.6	0.35	0.02	2.78	0.05	1.98	0.01	0.44	0.01	0.43	0.02	0.53	0.02
45.8	17.6	0.37	0.02	2.68	0.05	1.89	0.03	0.43	0.02	0.46	0.04	0.57	0.05
46.6	17.6	0.38	0.01	2.56	0.03	1.77	0.06	0.44	0.02	0.50	0.03	0.64	0.03
47.5	17.6	0.38	0.01	2.40	0.03	1.61	0.06	0.46	0.02	0.52	0.04	0.67	0.03
48.3	17.6	0.37	0.02	2.21	0.01	1.47	0.06	0.49	0.02	0.57	0.04	0.69	0.05
49.2	17.6	0.33	0.03	2.01	0.03	1.31	0.05	0.55	0.04	0.60	0.05	0.74	0.05
50.0	17.6	0.19	0.07	1.85	0.08	1.06	0.13	0.49	0.11	0.61	0.04	0.74	0.09

TABLE A7

The Sauter Mean Diameter, Number Density, and Volume Flux of the Fuel Droplets

Axial coordinate (mm)	Radial coordinate (mm)	Uncertainty (mm)	Sauter mean diameter (μm)	Type A uncertainty (μm)	Number density (droplets/cubic cm)	Type A uncertainty (droplets/cubic cm)	Volume flux (cm/s)	Type A uncertainty (cm/s)	Spray angle (degrees)
5.0	−0.36	0.19	34.00	0.50	1181	210	0.0063	0.0005	−4.1
5.0	0.27	0.19	34.38	0.57	1386	245	0.0073	0.0005	3.1
5.0	0.91	0.19	33.65	0.46	1631	222	0.0099	0.0005	10.3
5.0	1.54	0.19	32.62	0.78	2141	297	0.0209	0.0010	17.2
5.0	2.00	0.19	30.99	0.49	2143	357	0.0312	0.0073	21.8
5.0	2.10	0.19	31.38	0.44	2615	285	0.0452	0.0073	22.8
5.0	2.18	0.19	39.49	0.62	2789	235	0.0968	0.0052	23.5
5.0	2.37	0.19	33.32	0.54	2582	472	0.0600	0.0149	25.4
5.0	2.43	0.19	42.40	0.70	3473	385	0.1692	0.0064	25.9
5.0	2.54	0.19	42.23	0.66	3297	261	0.1693	0.0061	26.9
5.0	2.69	0.19	43.30	0.12	3854	593	0.2127	0.0212	28.3
5.0	2.76	0.19	41.41	0.86	2984	494	0.1446	0.0226	28.9
5.0	2.79	0.19	41.63	0.27	3317	478	0.1637	0.0142	29.2
5.0	2.81	0.19	41.00	1.13	3389	487	0.1554	0.0106	29.4
5.0	2.94	0.19	42.37	0.18	3608	245	0.1780	0.0068	30.5
5.0	3.05	0.19	41.43	0.37	2343	223	0.1115	0.0061	31.4
5.0	3.19	0.19	42.80	1.03	2160	150	0.1094	0.0031	32.6
5.0	3.23	0.19	46.92	0.82	1365	195	0.0952	0.0112	32.9
5.0	3.30	0.19	42.63	0.29	1433	59	0.0628	0.0013	33.4
5.0	3.45	0.19	41.28	1.55	1353	124	0.0446	0.0098	34.6
5.0	3.56	0.19	42.60	0.20	784	30	0.0305	0.0015	35.4
5.0	3.70	0.19	43.63	0.37	792	76	0.0317	0.0014	36.5
5.0	3.75	0.19	44.95	1.54	501	89	0.0230	0.0041	36.9
5.0	3.81	0.19	41.73	0.41	401	14	0.0139	0.0007	37.3
5.0	4.06	0.19	40.87	0.58	197	4	0.0057	0.0001	39.1
5.0	4.08	0.19	30.68	0.67	476	59	0.0038	0.0002	39.2
5.0	4.30	0.20	39.24	1.61	279	62	0.0046	0.0006	40.7
5.0	4.72	0.20	29.72	0.80	116	16	0.0006	0.0000	43.3
5.0	4.87	0.20	30.34	2.13	134	65	0.0007	0.0002	44.3
5.0	5.46	0.21	27.97	0.84	43	12	0.0001	0.0000	47.5
15.0	2.00	0.19	37.99	0.93	218	41	0.0010	0.0001	7.6
15.0	2.37	0.19	37.30	0.50	259	18	0.0012	0.0000	9.0
15.0	3.23	0.19	36.06	0.85	302	48	0.0015	0.0002	12.2
15.0	4.30	0.19	32.94	0.50	553	62	0.0032	0.0002	16.0
15.0	5.23	0.19	34.80	0.26	1186	59	0.0124	0.0007	19.2

TABLE A7

(Continued)

Axial coordinate (mm)	Radial coordinate (mm)	Uncertainty (mm)	Sauter mean diameter (μm)	Type A uncertainty (μm)	Number density (droplets/cubic cm)	Type A uncertainty (droplets/cubic cm)	Volume flux (cm/s)	Type A uncertainty (cm/s)	Spray angle (degrees)
15.0	5.46	0.19	32.60	0.33	1235	124	0.0110	0.0008	20.0
15.0	5.87	0.19	37.27	0.52	1912	113	0.0289	0.0011	21.4
15.0	6.05	0.20	35.10	0.49	1865	130	0.0234	0.0016	22.0
15.0	6.50	0.20	42.14	0.48	2426	166	0.0627	0.0013	23.4
15.0	6.66	0.20	41.03	0.72	1933	223	0.0487	0.0032	23.9
15.0	7.14	0.20	47.52	0.38	2681	179	0.1146	0.0045	25.4
15.0	7.27	0.20	44.65	0.47	2716	207	0.0959	0.0046	25.8
15.0	7.77	0.21	50.48	0.31	2858	165	0.1586	0.0059	27.4
15.0	7.88	0.21	51.01	0.58	2251	242	0.1402	0.0070	27.7
15.0	8.41	0.22	52.81	0.51	2181	78	0.1492	0.0084	29.3
15.0	8.49	0.22	52.24	0.41	2193	190	0.1465	0.0057	29.5
15.0	8.91	0.23	53.90	0.20	2460	12	0.1666	0.0059	30.7
15.0	9.11	0.23	54.98	0.55	1369	131	0.1125	0.0064	31.3
15.0	9.17	0.23	54.60	0.40	20.62	9	0.1466	0.0007	31.4
15.0	9.40	0.23	53.80	0.40	1497	52	0.1008	0.0017	32.1
15.0	9.42	0.23	54.55	0.90	1752	35	0.1240	0.0030	32.1
15.0	9.65	0.24	53.45	0.50	1238	75	0.0789	0.0006	32.8
15.0	9.91	0.24	53.60	1.40	974	16	0.0646	0.0017	33.4
15.0	9.93	0.24	54.85	0.70	1126	48	0.0782	0.0001	33.5
15.0	10.35	0.25	55.17	0.54	514	77	0.0382	0.0039	34.6
15.0	10.41	0.25	53.55	0.10	577	38	0.0363	0.0040	34.8
15.0	11.60	0.28	52.71	0.83	121	22	0.0068	0.0010	37.7
15.0	12.86	0.32	47.28	0.62	51	14	0.0013	0.0003	40.6
15.0	14.11	0.37	44.37	0.77	18	7	0.0003	0.0001	43.3
25.0	6.66	0.19	38.60	0.00	26	0	0.0002	0.0000	14.9
25.0	7.88	0.20	36.70	0.83	90	18	0.0006	0.0001	17.5
25.0	9.11	0.21	36.40	0.72	212	50	0.0019	0.0003	20.0
25.0	10.35	0.22	37.27	0.54	520	75	0.0062	0.0009	22.5
25.0	10.82	0.23	39.45	0.30	646	34	0.0100	0.0006	23.4
25.0	11.60	0.24	39.45	0.60	990	107	0.0161	0.0019	24.9
25.0	12.09	0.24	45.25	0.30	1189	36	0.0327	0.0010	25.8
25.0	12.86	0.26	45.81	0.49	1394	118	0.0423	0.0029	27.2
25.0	13.36	0.27	49.73	0.58	1488	90	0.0632	0.0017	28.1
25.0	14.11	0.28	50.64	0.44	1439	92	0.0685	0.0029	29.4
25.0	14.63	0.29	53.63	0.37	1401	69	0.0825	0.0035	30.3

TABLE A7

(Continued)

Axial coordinate (mm)	Radial coordinate (mm)	Uncertainty (mm)	Sauter mean diameter (μm)	Type A uncertainty (μm)	Number density (droplets/cubic cm)	Type A uncertainty (droplets/cubic cm)	Volume flux (cm/s)	Type A uncertainty (cm/s)	Spray angle (degrees)
25.0	15.27	0.31	55.15	0.10	1274	31	0.0863	0.0020	31.4
25.0	15.37	0.31	54.66	0.35	1119	73	0.0733	0.0030	31.6
25.0	15.88	0.32	55.85	0.30	950	60	0.0690	0.0020	32.4
25.0	16.54	0.34	57.15	0.50	782	7	0.0626	0.0011	33.5
25.0	16.63	0.35	56.69	0.35	665	63	0.0497	0.0033	33.6
25.0	17.15	0.36	57.55	0.10	480	5	0.0400	0.0004	34.4
25.0	17.81	0.38	58.00	0.00	374	10	0.0311	0.0009	35.5
25.0	17.89	0.38	58.15	0.37	306	33	0.0247	0.0023	35.6
25.0	18.42	0.40	57.65	0.70	210	22	0.0168	0.0014	36.4
25.0	19.15	0.43	57.48	0.72	127	18	0.0091	0.0007	37.5
25.0	20.42	0.48	56.46	0.55	56	9	0.0034	0.0004	39.2
25.0	21.68	0.53	53.66	0.75	33	6	0.0013	0.0002	40.9
25.0	22.95	0.59	52.80	0.81	18	3	0.0006	0.0001	42.5
35.0	9.11	0.20	37.90	0.00	15	0	0.0001	0.0000	14.6
35.0	10.35	0.21	38.70	0.00	28	0	0.0002	0.0000	16.5
35.0	11.60	0.22	38.70	0.40	56	7	0.0005	0.0001	18.3
35.0	12.86	0.23	39.82	0.25	136	15	0.0017	0.0002	20.2
35.0	14.11	0.25	41.21	0.30	277	36	0.0043	0.0006	22.0
35.0	15.37	0.27	43.99	0.29	456	60	0.0098	0.0012	23.7
35.0	15.78	0.27	47.00	0.31	514	56	0.0147	0.0016	24.3
35.0	16.42	0.28	51.10	0.20	424	0	0.0186	0.0000	25.1
35.0	16.63	0.29	46.89	0.20	717	72	0.0210	0.0020	25.4
35.0	17.05	0.30	49.23	0.53	756	47	0.0277	0.0010	26.0
35.0	17.15	0.30	51.50	0.20	719	4	0.0317	0.0007	26.1
35.0	17.69	0.31	52.35	2.30	661	171	0.0335	0.0022	26.8
35.0	17.89	0.32	49.18	0.48	911	65	0.0332	0.0028	27.1
35.0	18.32	0.33	52.37	0.66	928	78	0.0446	0.0021	27.6
35.0	18.42	0.33	53.70	0.00	872	3	0.0475	0.0018	27.8
35.0	18.96	0.34	55.00	0.60	811	180	0.0491	0.0059	28.4
35.0	19.15	0.35	52.92	0.28	922	53	0.0463	0.0021	28.7
35.0	19.59	0.36	54.23	0.52	929	79	0.0510	0.0028	29.2
35.0	19.69	0.36	55.85	0.50	879	18	0.0556	0.0019	29.4
35.0	20.23	0.37	56.20	0.40	751	157	0.0510	0.0059	30.0
35.0	20.42	0.38	54.99	0.29	754	61	0.0451	0.0023	30.3
35.0	20.86	0.39	56.37	0.66	703	53	0.0457	0.0029	30.8

TABLE A7

(Continued)

Axial coordinate (mm)	Radial coordinate (mm)	Uncertainty (mm)	Sauter mean diameter (μm)	Type A uncertainty (μm)	Number density (droplets/cubic cm)	Type A uncertainty (droplets/cubic cm)	Volume flux (cm/s)	Type A uncertainty (cm/s)	Spray angle (degrees)
35.0	20.96	0.39	57.05	0.70	681	4	0.0491	0.0017	30.9
35.0	21.50	0.41	58.25	0.10	488	7	0.0398	0.0018	31.6
35.0	21.68	0.42	57.61	0.29	481	42	0.0348	0.0025	31.8
35.0	22.23	0.43	58.40	0.00	441	9	0.0349	0.0009	32.4
35.0	22.77	0.45	59.80	0.20	309	13	0.0269	0.0014	33.0
35.0	22.95	0.46	59.43	0.20	281	28	0.0231	0.0020	33.3
35.0	23.50	0.47	59.20	0.00	246	5	0.0205	0.0004	33.9
35.0	24.21	0.50	60.04	0.22	150	16	0.0126	0.0012	34.7
35.0	25.48	0.55	60.51	0.37	79	8	0.0064	0.0005	36.1
35.0	26.74	0.59	59.97	0.57	41	5	0.0029	0.0003	37.4
35.0	28.01	0.65	59.27	0.24	23	6	0.0014	0.0004	38.7
45.0	14.11	0.23	40.20	0.00	11	0	0.0001	0.0000	17.4
45.0	15.37	0.24	40.40	0.00	19	0	0.0002	0.0000	18.9
45.0	16.63	0.26	41.90	0.00	38	0	0.0005	0.0000	20.3
45.0	16.93	0.26	43.67	0.44	43	3	0.0007	0.0000	20.6
45.0	17.89	0.28	42.98	0.19	77	17	0.0013	0.0003	21.7
45.0	18.84	0.29	46.00	0.40	81	4	0.0020	0.0001	22.7
45.0	19.15	0.30	44.07	0.52	161	28	0.0032	0.0005	23.1
45.0	19.47	0.31	46.77	0.24	160	11	0.0040	0.0002	23.4
45.0	19.69	0.31	49.20	1.20	116	1	0.0040	0.0003	23.6
45.0	20.11	0.32	47.20	0.40	149	1	0.0043	0.0002	24.1
45.0	20.42	0.33	46.79	0.39	205	31	0.0054	0.0006	24.4
45.0	20.96	0.34	50.10	0.00	199	3	0.0078	0.0002	25.0
45.0	21.38	0.35	48.70	0.20	261	2	0.0084	0.0002	25.4
45.0	21.68	0.35	48.07	0.33	384	19	0.0117	0.0001	25.7
45.0	22.01	0.36	49.30	0.53	391	31	0.0132	0.0008	26.1
45.0	22.23	0.37	52.00	0.00	310	2	0.0142	0.0001	26.3
45.0	22.95	0.38	50.10	0.41	441	34	0.0163	0.0012	27.0
45.0	23.28	0.39	50.67	0.75	540	50	0.0205	0.0009	27.4
45.0	24.21	0.42	51.52	0.40	510	27	0.0223	0.0012	28.3
45.0	24.55	0.42	51.73	0.47	590	51	0.0258	0.0009	28.6
45.0	25.48	0.45	53.05	0.50	509	31	0.0251	0.0012	29.5
45.0	25.82	0.46	54.33	0.85	540	74	0.0293	0.0017	29.8
45.0	26.46	0.48	54.70	0.20	462	15	0.0271	0.0004	30.5
45.0	26.74	0.49	55.27	0.32	435	33	0.0258	0.0014	30.7

TABLE A7

(Continued)

Axial coordinate (mm)	Radial coordinate (mm)	Uncertainty (mm)	Sauter mean diameter (μm)	Type A uncertainty (μm)	Number density (droplets/cubic cm)	Type A uncertainty (droplets/cubic cm)	Volume flux (cm/s)	Type A uncertainty (cm/s)	Spray angle (degrees)
45.0	27.31	0.51	56.55	0.10	362	3	0.0260	0.0020	31.2
45.0	27.73	0.52	56.50	0.00	369	9	0.0250	0.0002	31.6
45.0	28.01	0.53	56.78	0.28	332	25	0.0217	0.0013	31.9
45.0	28.58	0.55	58.40	0.20	272	0	0.0209	0.0000	32.4
45.0	29.00	0.56	57.85	0.10	279	3	0.0206	0.0007	32.8
45.0	29.28	0.57	58.04	0.27	220	17	0.0162	0.0011	33.0
45.0	29.85	0.59	59.20	0.20	184	2	0.0150	0.0001	33.6
45.0	30.27	0.61	58.65	0.50	187	8	0.0142	0.0002	33.9
45.0	30.55	0.62	58.86	0.42	140	11	0.0108	0.0007	34.2
45.0	31.12	0.64	59.60	0.40	122	2	0.0099	0.0002	34.7
45.0	31.81	0.67	59.56	0.49	86	9	0.0066	0.0006	35.3
45.0	33.08	0.72	59.92	0.90	52	8	0.0037	0.0004	36.3
45.0	34.35	0.77	60.70	0.73	35	3	0.0024	0.0002	37.4
45.0	35.62	0.82	59.80	0.69	23	3	0.0013	0.0001	38.4
45.0	36.88	0.88	59.68	0.76	18	2	0.0009	0.0001	39.3
55.0	17.89	0.26	43.20	0.00	6	0	0.0001	0.0000	18.0
55.0	19.15	0.27	42.80	0.00	11	0	0.0001	0.0000	19.2
55.0	20.42	0.29	43.90	0.00	21	0	0.0003	0.0000	20.4
55.0	21.68	0.31	44.75	0.59	44	5	0.0008	0.0001	21.5
55.0	21.89	0.32	46.13	0.37	42	2	0.0009	0.0000	21.7
55.0	22.95	0.34	46.20	0.96	73	19	0.0017	0.0004	22.6
55.0	23.16	0.34	47.57	0.77	76	5	0.0019	0.0001	22.8
55.0	24.21	0.36	47.57	0.32	101	16	0.0026	0.0004	23.8
55.0	24.43	0.37	48.57	0.18	128	7	0.0036	0.0001	23.9
55.0	25.48	0.39	48.90	0.67	176	25	0.0054	0.0010	24.9
55.0	25.70	0.40	49.97	0.52	201	9	0.0065	0.0001	25.0
55.0	26.74	0.42	50.08	0.37	225	21	0.0079	0.0008	25.9
55.0	26.97	0.43	50.80	0.95	279	28	0.0101	0.0002	26.1
55.0	28.01	0.45	51.98	1.09	290	30	0.0121	0.0009	27.0
55.0	28.24	0.46	52.00	0.46	334	40	0.0139	0.0010	27.2
55.0	29.28	0.49	52.52	0.62	327	24	0.0147	0.0007	28.0
55.0	29.51	0.50	53.50	0.64	348	55	0.0163	0.0015	28.2
55.0	30.55	0.53	54.43	0.88	310	42	0.0166	0.0011	29.0
55.0	30.78	0.53	55.13	0.93	304	37	0.0173	0.0003	29.2
55.0	31.81	0.56	55.40	0.39	286	15	0.0167	0.0005	30.0

TABLE A7

(Continued)

Axial coordinate (mm)	Radial coordinate (mm)	Uncertainty (mm)	Sauter mean diameter (μm)	Type A uncertainty (μm)	Number density (droplets/cubic cm)	Type A uncertainty (droplets/cubic cm)	Volume flux (cm/s)	Type A uncertainty (cm/s)	Spray angle (degrees)
55.0	32.05	0.57	56.10	0.53	277	26	0.0166	0.0002	30.2
55.0	33.08	0.61	56.92	0.75	215	22	0.0143	0.0010	31.0
55.0	33.32	0.61	57.03	0.70	221	18	0.0148	0.0002	31.2
55.0	33.95	0.63	58.20	0.20	200	3	0.0148	0.0003	31.7
55.0	34.35	0.65	57.40	0.47	181	12	0.0123	0.0006	32.0
55.0	34.93	0.67	59.75	0.30	153	1	0.0124	0.0003	32.4
55.0	35.22	0.68	59.30	0.00	157	3	0.0121	0.0001	32.6
55.0	35.62	0.69	59.60	0.38	117	10	0.0089	0.0005	32.9
55.0	36.20	0.71	60.20	0.00	111	1	0.0091	0.0001	33.3
55.0	36.49	0.72	59.90	0.20	123	0	0.0094	0.0001	33.6
55.0	36.88	0.74	60.32	0.33	92	6	0.0070	0.0004	33.8
55.0	37.47	0.76	60.85	0.30	78	0	0.0064	0.0002	34.3
55.0	38.15	0.79	61.64	0.37	61	4	0.0046	0.0003	34.7
55.0	39.42	0.84	61.53	0.40	45	4	0.0032	0.0003	35.6
55.0	40.69	0.89	62.37	0.68	32	1	0.0020	0.0001	36.5
55.0	41.96	0.95	61.58	0.92	24	3	0.0013	0.0002	37.3
55.0	43.23	1.00	62.27	1.00	15	1	0.0008	0.0001	38.2
65.0	24.21	0.33	42.70	0.00	11	0	0.0002	0.0000	20.4
65.0	25.48	0.35	43.40	0.00	21	0	0.0003	0.0000	21.4
65.0	26.74	0.38	45.85	0.25	40	5	0.0008	0.0001	22.4
65.0	28.01	0.40	46.63	0.37	66	8	0.0015	0.0001	23.3
65.0	29.28	0.43	47.43	0.25	106	11	0.0026	0.0002	24.2
65.0	30.02	0.45	50.50	0.20	90	11	0.0029	0.0002	24.8
65.0	30.55	0.46	49.10	0.42	140	15	0.0041	0.0002	25.2
65.0	31.12	0.48	51.75	0.50	140	21	0.0051	0.0002	25.6
65.0	31.29	0.48	50.95	0.70	130	14	0.0045	0.0002	25.7
65.0	31.81	0.50	50.33	0.41	178	16	0.0059	0.0004	26.1
65.0	32.39	0.51	52.55	0.70	186	23	0.0075	0.0004	26.5
65.0	32.56	0.52	52.25	0.30	171	17	0.0070	0.0003	26.6
65.0	33.08	0.53	51.50	0.53	207	16	0.0079	0.0003	27.0
65.0	33.66	0.55	53.90	0.20	209	4	0.0099	0.0002	27.4
65.0	33.83	0.55	52.95	0.90	209	23	0.0090	0.0004	27.5
65.0	34.35	0.57	52.38	0.38	225	12	0.0095	0.0006	27.9
65.0	34.93	0.58	54.65	0.10	232	18	0.0120	0.0004	28.2
65.0	35.10	0.59	53.90	0.40	228	42	0.0109	0.0006	28.4

TABLE A7

(Continued)

Axial coordinate (mm)	Radial coordinate (mm)	Uncertainty (mm)	Sauter mean diameter (μm)	Type A uncertainty (μm)	Number density (droplets/cubic cm)	Type A uncertainty (droplets/cubic cm)	Volume flux (cm/s)	Type A uncertainty (cm/s)	Spray angle (degrees)
65.0	35.62	0.60	53.94	0.70	226	13	0.0108	0.0003	28.7
65.0	36.20	0.62	55.35	0.30	246	4	0.0133	0.0000	29.1
65.0	36.37	0.63	56.10	0.40	210	41	0.0117	0.0011	29.2
65.0	36.88	0.64	55.27	0.74	210	19	0.0112	0.0005	29.6
65.0	37.47	0.66	57.60	0.40	196	4	0.0129	0.0006	30.0
65.0	37.64	0.67	56.75	0.70	198	34	0.0118	0.0007	30.1
65.0	38.15	0.68	56.23	0.71	181	16	0.0105	0.0005	30.4
65.0	38.74	0.70	58.20	0.20	173	3	0.0118	0.0003	30.8
65.0	38.91	0.71	57.20	0.40	177	26	0.0110	0.0013	30.9
65.0	39.42	0.72	57.61	0.62	156	12	0.0097	0.0005	31.2
65.0	40.01	0.75	58.45	0.30	146	5	0.0099	0.0001	31.6
65.0	40.18	0.75	58.75	0.50	147	17	0.0098	0.0008	31.7
65.0	40.69	0.77	59.07	0.35	125	10	0.0082	0.0005	32.0
65.0	41.28	0.79	60.20	0.60	118	4	0.0085	0.0000	32.4
65.0	41.45	0.80	59.20	0.60	122	15	0.0081	0.0005	32.5
65.0	41.96	0.82	59.74	0.41	97	8	0.0065	0.0003	32.8
65.0	42.55	0.84	60.50	0.20	90	2	0.0065	0.0002	32.2
65.0	42.72	0.84	60.25	0.50	91	7	0.0063	0.0003	33.3
65.0	43.23	0.86	60.52	0.72	74	7	0.0049	0.0003	33.6
65.0	43.82	0.89	61.05	0.30	69	2	0.0048	0.0001	34.0
65.0	44.49	0.91	61.37	0.41	58	5	0.0038	0.0002	34.4
65.0	45.76	0.96	61.46	0.49	45	6	0.0027	0.0002	35.1
65.0	47.03	1.02	62.07	0.35	32	3	0.0019	0.0002	35.9
65.0	48.30	1.07	62.37	0.27	24	3	0.0013	0.0002	36.6
65.0	49.57	1.13	63.03	0.40	16	1	0.0009	0.0001	37.3

TABLE A8

Mean Axial and Radial Velocity Components of the Fuel Droplets

Radial coordinate (mm)	Axial coordinate (mm)	Axial velocity (m/s)	Type A uncertainty (m/s)	Radial velocity (m/s)	Type A uncertainty (m/s)
0.00	5	5.46	0.37	0.47	0.23
0.27	5	3.57	0.27	0.34	0.05
0.64	5	4.57	0.75	0.93	0.15
0.91	5	5.79	0.28	1.06	0.10
1.27	5	5.59	0.41	1.51	0.20
1.54	5	11.30	0.37	3.26	0.12
1.91	5	8.28	0.25	2.65	0.14
2.00	5	15.80	1.22	0.23	0.16
2.10	5	17.40	0.93	−0.06	0.74
2.18	5	19.60	0.13	8.57	0.15
2.37	5	18.70	1.05	3.93	0.20
2.43	5	21.30	0.03	10.20	0.03
2.54	5	22.10	0.10	11.00	0.17
2.69	5	22.00	0.16	11.90	0.14
2.76	5	21.80	0.48	7.11	0.23
2.79	5	22.10	0.02	12.30	0.08
2.81	5	21.30	0.16	12.80	0.10
2.94	5	21.30	0.13	12.60	0.05
3.05	5	21.10	0.06	13.00	0.03
3.18	5	21.40	0.21	11.60	0.16
3.20	5	20.10	0.06	13.10	0.09
3.23	5	21.80	0.22	10.20	0.20
3.30	5	19.50	0.04	13.20	0.03
3.45	5	17.30	0.57	12.60	0.23
3.56	5	17.90	0.07	13.20	0.10
3.70	5	16.80	0.21	12.90	0.16
3.75	5	18.40	0.76	11.40	0.28
3.81	5	16.30	0.06	12.90	0.06
4.06	5	14.70	0.03	12.60	0.04
4.08	5	11.60	0.13	10.30	0.07
4.30	5	13.70	0.64	11.20	0.41
4.45	5	17.40	0.13	14.20	0.11
4.72	5	8.59	0.18	8.94	0.16
4.87	5	9.50	1.12	9.71	0.78
5.08	5	14.20	0.12	13.60	0.13
5.46	5	6.74	0.40	8.44	0.29
10.20	15	18.50	1.06	12.20	0.55
10.40	15	15.90	0.19	10.30	0.14
10.40	15	15.00	0.04	9.83	0.01
11.40	15	16.00	1.08	11.90	0.72
11.60	15	13.10	0.25	9.73	0.19
12.70	15	13.20	0.84	11.00	0.61
12.90	15	9.60	0.27	8.25	0.20
14.10	15	7.21	0.24	7.13	0.24
2.00	15	3.79	0.18	0.49	0.07
2.37	15	3.90	0.11	0.68	0.08
2.54	15	0.99	0.13	0.09	0.07
3.23	15	5.25	0.12	1.11	0.05
3.81	15	4.71	0.19	1.15	0.04
4.30	15	8.09	0.12	2.15	0.05
5.08	15	9.84	0.12	3.30	0.09
5.23	15	12.00	0.09	4.06	0.04
5.46	15	11.80	0.16	3.94	0.07
5.72	15	12.00	0.09	4.06	0.04

TABLE A8

(Continued)

Radial coordinate (mm)	Axial coordinate (mm)	Axial velocity (m/s)	Type A uncertainty (m/s)	Radial velocity (m/s)	Type A uncertainty (m/s)
5.87	15	14.00	0.07	5.43	0.03
6.06	15	13.70	0.20	5.05	0.07
6.35	15	15.40	0.06	6.37	0.04
6.50	15	16.00	0.11	6.92	0.05
6.66	15	16.20	0.29	6.56	0.11
6.99	15	16.00	0.11	6.92	0.05
7.14	15	17.70	0.08	8.40	0.05
7.27	15	17.40	0.21	7.71	0.07
7.62	15	19.40	0.63	9.73	0.44
7.77	15	18.10	0.08	9.36	0.06
7.88	15	19.00	0.23	9.11	0.11
8.26	15	18.10	0.08	9.36	0.06
8.41	15	18.30	0.16	10.00	0.10
8.49	15	18.60	0.11	9.65	0.07
8.89	15	20.30	0.32	11.80	0.15
8.92	15	17.30	0.07	9.84	0.03
9.11	15	18.40	0.19	10.30	0.11
9.17	15	17.10	0.14	9.92	0.11
9.40	15	16.80	0.13	9.98	0.02
9.42	15	16.70	0.05	9.98	0.03
9.65	15	16.30	0.10	9.93	0.08
9.91	15	16.00	0.15	9.99	0.05
9.93	15	15.80	0.14	10.00	0.08
10.40	25	10.50	0.26	3.51	0.11
10.80	25	11.30	0.09	4.37	0.08
11.40	25	11.30	0.09	4.37	0.08
11.60	25	12.10	0.26	4.74	0.11
12.10	25	13.60	0.04	5.90	0.04
12.70	25	13.60	0.04	5.90	0.04
12.90	25	14.30	0.19	6.26	0.10
13.40	25	15.00	0.12	7.27	0.07
14.00	25	15.00	0.12	7.27	0.07
14.10	25	15.50	0.20	7.54	0.11
14.60	25	15.70	0.07	8.30	0.04
15.20	25	15.70	0.07	8.30	0.04
15.30	25	15.60	0.17	8.38	0.12
15.40	25	15.90	0.11	8.43	0.07
15.90	25	15.60	0.12	8.59	0.07
16.50	25	15.20	0.00	8.84	0.01
16.60	25	15.30	0.13	8.82	0.07
17.20	25	14.80	0.09	8.84	0.04
17.80	25	14.00	0.02	8.88	0.03
17.90	25	14.30	0.14	8.94	0.07
18.40	25	13.50	0.06	8.73	0.07
19.20	25	12.50	0.25	8.60	0.15
20.40	25	10.70	0.16	8.01	0.10
21.70	25	8.67	0.18	7.12	0.12
23.00	25	7.17	0.17	6.42	0.19
10.40	35	6.02	0.00	0.93	0.00
11.60	35	7.07	0.14	1.71	0.02
12.90	35	8.57	0.17	2.57	0.05
14.10	35	9.72	0.15	3.40	0.05
15.40	35	11.00	0.11	4.31	0.06
15.80	35	11.90	0.06	4.92	0.07

TABLE A8

(Continued)

Radial coordinate (mm)	Axial coordinate (mm)	Axial velocity (m/s)	Type A uncertainty (m/s)	Radial velocity (m/s)	Type A uncertainty (m/s)
16.40	35	13.20	0.02	5.64	0.03
16.50	35	11.90	0.06	4.92	0.07
16.60	35	12.30	0.10	5.26	0.06
17.10	35	12.90	0.19	5.81	0.02
17.20	35	13.50	0.12	5.93	0.08
17.70	35	13.80	0.48	6.38	0.20
17.80	35	12.90	0.19	5.81	0.02
17.90	35	13.00	0.19	6.01	0.13
18.30	35	13.70	0.20	6.66	0.06
18.40	35	14.10	0.01	6.69	0.01
19.00	35	14.20	0.36	7.03	0.16
19.10	35	13.70	0.20	6.66	0.06
19.20	35	13.90	0.08	6.89	0.05
19.60	35	13.90	0.11	7.18	0.01
19.70	35	14.40	0.06	7.31	0.02
20.20	35	14.20	0.42	7.53	0.14
20.30	35	13.90	0.11	7.18	0.01
20.40	35	14.00	0.10	7.41	0.05
20.90	35	13.90	0.15	7.68	0.03
21.00	35	14.20	0.03	7.67	0.00
21.50	35	14.10	0.16	7.92	0.11
21.60	35	13.90	0.15	7.68	0.03
21.70	35	14.00	0.09	7.84	0.04
22.20	35	13.90	0.03	7.97	0.03
22.80	35	13.70	0.12	8.14	0.07
23.00	35	13.50	0.11	8.04	0.05
23.50	35	13.10	0.06	7.98	0.06
24.20	35	12.60	0.12	7.98	0.05
25.50	35	11.40	0.11	7.72	0.05
26.70	35	10.10	0.17	7.25	0.12
28.00	35	8.79	0.03	6.70	0.04
14.10	45	5.37	0.00	0.81	0.00
15.40	45	6.42	0.00	1.35	0.00
16.60	45	7.28	0.00	1.96	0.00
16.90	45	8.21	0.12	2.45	0.04
17.80	45	8.21	0.12	2.45	0.04
17.90	45	8.52	0.09	2.66	0.04
18.80	45	9.69	0.03	3.37	0.02
19.20	45	9.52	0.20	3.36	0.07
19.50	45	10.00	0.07	3.78	0.02
19.70	45	10.90	0.34	3.97	0.14
20.10	45	10.40	0.16	3.98	0.06
20.30	45	10.00	0.07	3.78	0.02
20.40	45	10.50	0.10	4.01	0.04
21.00	45	11.70	0.03	4.61	0.01
21.40	45	11.20	0.04	4.62	0.02
21.70	45	11.30	0.07	4.73	0.06
22.00	45	11.50	0.15	5.00	0.04
22.20	45	12.30	0.01	5.25	0.03
22.90	45	11.50	0.15	5.00	0.04
23.00	45	11.90	0.14	5.27	0.07
23.30	45	11.90	0.24	5.55	0.08
24.10	45	11.90	0.24	5.55	0.08
24.20	45	12.40	0.12	5.84	0.07

TABLE A8

(Continued)

Radial coordinate (mm)	Axial coordinate (mm)	Axial velocity (m/s)	Type A uncertainty (m/s)	Radial velocity (m/s)	Type A uncertainty (m/s)
24.60	45	12.30	0.13	6.02	0.06
25.40	45	12.30	0.13	6.02	0.06
25.50	45	12.70	0.13	6.28	0.07
25.80	45	12.80	0.26	6.57	0.08
26.50	45	12.80	0.13	6.63	0.05
26.70	45	12.80	0.26	6.57	0.08
26.70	45	12.90	0.08	6.73	0.04
27.30	45	13.20	0.06	6.95	0.01
27.70	45	12.70	0.00	6.95	0.00
28.00	45	12.80	0.09	7.01	0.03
28.60	45	12.90	0.06	7.17	0.01
29.00	45	12.40	0.00	7.11	0.01
29.30	45	12.40	0.08	7.16	0.03
29.90	45	12.30	0.08	7.20	0.03
30.30	45	11.80	0.03	7.11	0.02
30.60	45	11.80	0.08	7.14	0.02
31.10	45	11.50	0.08	7.06	0.04
31.80	45	10.90	0.13	6.96	0.06
33.10	45	9.93	0.18	6.63	0.06
34.40	45	9.04	0.15	6.31	0.11
35.60	45	7.98	0.14	5.83	0.15
36.90	45	7.06	0.13	5.39	0.07
17.90	55	6.13	0.00	1.12	0.00
19.20	55	6.63	0.00	1.56	0.00
20.40	55	7.50	0.00	2.07	0.00
21.70	55	8.39	0.20	2.64	0.08
21.90	55	8.57	0.07	2.78	0.04
22.90	55	8.57	0.07	2.78	0.04
23.00	55	9.11	0.26	3.13	0.12
23.20	55	9.36	0.05	3.31	0.10
24.10	55	9.36	0.05	3.31	0.10
24.20	55	9.65	0.07	3.55	0.04
24.40	55	9.93	0.07	3.80	0.07
25.40	55	9.93	0.07	3.80	0.07
25.50	55	10.30	0.24	4.09	0.14
25.70	55	10.50	0.08	4.29	0.06
26.70	55	10.50	0.08	4.29	0.06
26.70	55	10.80	0.10	4.52	0.07
27.00	55	10.90	0.12	4.70	0.05
27.90	55	10.90	0.12	4.70	0.05
28.00	55	11.60	0.33	5.11	0.17
28.20	55	11.30	0.10	5.17	0.08
29.20	55	11.30	0.10	5.17	0.08
29.30	55	11.60	0.17	5.39	0.09
29.50	55	11.70	0.20	5.58	0.02
30.50	55	11.70	0.20	5.58	0.02
30.60	55	12.00	0.23	5.86	0.12
30.80	55	12.00	0.18	5.97	0.06
31.80	55	12.00	0.18	5.97	0.06
31.80	55	12.00	0.11	6.08	0.06
32.10	55	11.90	0.18	6.18	0.08
33.00	55	11.90	0.18	6.18	0.08
33.10	55	11.90	0.13	6.30	0.07
33.30	55	11.70	0.19	6.31	0.11

TABLE A8

(Continued)

Radial coordinate (mm)	Axial coordinate (mm)	Axial velocity (m/s)	Type A uncertainty (m/s)	Radial velocity (m/s)	Type A uncertainty (m/s)
34.00	55	11.70	0.06	6.33	0.04
34.30	55	11.70	0.19	6.31	0.11
34.40	55	11.40	0.10	6.31	0.05
34.90	55	11.60	0.08	6.38	0.05
35.20	55	11.20	0.04	6.33	0.02
35.60	55	11.00	0.09	6.36	0.05
36.20	55	11.00	0.06	6.29	0.05
36.50	55	10.50	0.03	6.21	0.03
36.90	55	10.40	0.08	6.24	0.05
37.50	55	10.30	0.06	6.14	0.05
38.20	55	9.70	0.05	6.05	0.06
39.40	55	8.83	0.09	5.70	0.07
40.70	55	8.09	0.15	5.36	0.11
42.00	55	7.25	0.19	4.99	0.17
43.20	55	6.78	0.09	4.72	0.03
24.20	65	7.01	0.00	1.71	0.00
25.50	65	7.47	0.00	2.06	0.00
26.70	65	8.25	0.21	2.56	0.08
28.00	65	8.75	0.15	2.90	0.06
29.30	65	9.16	0.07	3.26	0.05
30.00	65	9.76	0.11	3.65	0.06
30.60	65	9.78	0.09	3.69	0.07
31.10	65	10.30	0.25	3.98	0.09
31.30	65	10.10	0.23	3.97	0.07
31.80	65	10.20	0.07	4.10	0.05
32.40	65	10.60	0.22	4.35	0.10
32.60	65	10.50	0.16	4.39	0.09
33.10	65	10.60	0.17	4.45	0.09
33.70	65	11.10	0.05	4.76	0.05
33.80	65	10.60	0.23	4.65	0.11
34.40	65	10.70	0.11	4.73	0.07
34.90	65	11.20	0.07	5.02	0.05
35.10	65	10.80	0.18	4.92	0.06
35.60	65	10.90	0.13	5.04	0.06
36.20	65	11.20	0.05	5.23	0.00
36.40	65	11.00	0.15	5.23	0.06
36.90	65	11.00	0.13	5.27	0.06
37.50	65	11.30	0.11	5.52	0.07
37.60	65	10.90	0.23	5.38	0.09
38.20	65	10.80	0.13	5.40	0.06
38.70	65	11.00	0.04	5.58	0.02
38.90	65	10.50	0.17	5.42	0.04
39.40	65	10.60	0.13	5.50	0.07
40.00	65	10.50	0.02	5.50	0.02
40.20	65	10.20	0.12	5.46	0.03
40.70	65	10.20	0.15	5.52	0.07
41.30	65	10.10	0.14	5.51	0.09
41.50	65	9.67	0.21	5.36	0.08
42.00	65	9.67	0.15	5.43	0.07
42.60	65	9.52	0.03	5.35	0.01
42.70	65	9.21	0.09	5.27	0.08
43.20	65	9.02	0.19	5.23	0.10
43.80	65	8.89	0.15	5.14	0.11
44.50	65	8.45	0.13	5.05	0.08

TABLE A8

(Continued)

Radial coordinate (mm)	Axial coordinate (mm)	Axial velocity (m/s)	Type A uncertainty (m/s)	Radial velocity (m/s)	Type A uncertainty (m/s)
45.80	65	7.77	0.22	4.78	0.11
47.00	65	7.27	0.10	4.59	0.07
48.30	65	6.68	0.13	4.35	0.07
49.60	65	6.41	0.14	4.13	0.09

TABLE A9

Concentration of Major Species in the Exhaust Gas

Radial coordinate (mm)	Polar angle (degrees)	Carbon monoxide mole fraction	Type A uncertainty	Carbon dioxide mole fraction	Type A uncertainty	Methanol mole fraction	Type A uncertainty
0.0	—	4.61E-04	2.9E-04	2.51E-02	3.8E-03	6.29E-03	5.8E-05
44.5	0	3.52E-04	5.1E-05	2.34E-02	2.3E-03	6.12E-03	8.0E-05
88.9	0	3.90E-04	4.8E-05	2.57E-02	3.9E-03	6.34E-03	1.7E-04
133.4	0	3.99E-04	3.7E-05	2.63E-02	4.5E-03	6.39E-03	4.2E-05
177.8	0	3.61E-04	3.9E-05	2.52E-02	4.3E-03	6.22E-03	5.2E-05
44.5	90	5.88E-04	6.2E-04	2.74E-02	4.2E-03	6.67E-03	5.4E-05
88.9	90	5.15E-04	3.4E-04	2.61E-02	3.7E-03	6.69E-03	2.4E-05
133.4	90	4.64E-04	1.9E-04	2.80E-02	4.2E-03	6.76E-03	3.2E-05
177.8	90	1.19E-03	3.1E-03	2.70E-02	3.7E-03	6.96E-03	3.1E-05
44.5	180	2.80E-04	5.0E-05	1.87E-02	1.1E-03	5.85E-03	8.0E-05
88.9	180	2.65E-04	7.0E-05	1.83E-02	1.2E-03	5.73E-03	4.3E-05
133.4	180	2.79E-04	8.2E-05	1.78E-02	1.5E-03	5.64E-03	4.0E-05
177.8	180	2.83E-04	6.0E-05	1.72E-02	1.1E-03	5.52E-03	7.4E-05